CK2 alpha prime and alpha-synuclein pathogenic functional interaction mediates inflammation and transcriptional dysregulation in Huntington's disease

Dahyun Yu[1,*], Nicole Zarate[1,*], Francesco Cuccu[1,3], Johnny S. Yue[1,4], Taylor G. Brown[1], Wei Tsai[1], Rachel Mansky[1], Kevin Jiang[1], Hyuck Kim[1#], Angel White[1], Carmen Nanclares[1], Tessa Nichols-Meade[1], Sarah N. Larson[2], Katie Gundry[2], Ying Zhang[5], Cristina Tomas-Zapico[6#], Jose J. Lucas[6,7], Michael Benneyworth[1], Gülin Öz[2], Marija Cvetanovic[1], Alfonso Araque[1] and Rocio Gomez-Pastor[1±].

[1]Department of Neuroscience, School of Medicine, University of Minnesota, Minneapolis, MN, United States. [2]Center for Magnetic Resonance Research. Department of Radiology, School of Medicine, University of Minnesota, Minneapolis, MN, United States. [3]Department of Life and Environment Sciences, University of Cagliari, Cagliari, Italy. [4] Mounds View High School, Arden Hills, Minnesota. [5]Minnesota Supercomputing Institute, University of Minnesota, Minneapolis, MN, United States. [6] Centro de Biología Molecular 'Severo Ochoa' (CBMSO) CSIC/UAM, Madrid, Spain. [7]Networking Research Center on Neurodegenerative Diseases (CIBERNED), Instituto de Salud Carlos III, Madrid, Spain

[#]Current address: HK, MEPSGEN, Seoul 05836, South Korea. CTZ, Department of Functional Biology, Physiology, University of Oviedo, Asturias 33006, Spain; Health Research Institute of the Principality of Asturias (ISPA), Asturias 33011, Spain.

[*]These authors contributed equally to the manuscript

[±]Correspondence should be addressed to Rocio Gomez-Pastor, University of Minnesota, 321 Church St. SE, Jackson Hall Room 6-145, Minneapolis, MN 55455, rgomezpa@umn.edu

Keywords: Huntington's disease, polyglutamine, CK2 alpha prime, alpha-synuclein, neuroinflammation, protein aggregation.

Abstract

Huntington's Disease (HD) is a neurodegenerative disorder caused by a CAG trinucleotide repeat expansion in the Htt gene for which no therapies are available. This mutation causes HTT protein misfolding and aggregation, preferentially affecting medium spiny neurons (MSNs) of the basal ganglia. Transcriptional perturbations in synaptic genes and neuroinflammation are key processes that precede MSN dysfunction and motor symptom onset. Understanding the interplay between these processes is crucial to develop effective therapeutic strategies to treat HD. We investigated whether protein kinase CK2α', a kinase upregulated in MSNs in HD and previously associated with Parkinson's disease (PD), participates in the regulation of neuroinflammation and synaptic function during HD progression. We used the heterozygous knock-in zQ175 HD mouse model that lacks one allele of CK2α' and performed cytokine proteome profiling, RNA-seq, electrophysiological recordings, and behavioral analyses. We showed that CK2α' haploinsufficiency in zQ175 mice ameliorated neuroinflammation, HTT aggregation, transcriptional alterations, excitatory synaptic transmission deficits, and motor dysfunction. Our RNA-seq analyses also revealed a connection between α-syn, a protein associated with PD, and the transcriptional perturbations mediated by CK2α' in HD. We found that CK2α' increased α-syn serine 129 phosphorylation (pS129-α-syn), a post-translational modification linked to α-synucleinopathy, and its accumulation in the nucleus of MSNs in zQ175 mice and in patients with HD. Our data demonstrated that CK2α' negatively contributes to HD by promoting striatal synucleinopathy, transcriptional alteration of synaptic genes and neuroinflammation. We propose CK2α' as a potential therapeutic target to treat HD.

Significance statement

Upregulation of Protein kinase CK2α' mediates neuroinflammation and transcriptional dysregulation of synaptic genes in the zQ175 mouse model of HD and its depletion improved several HD-like phenotypes in this mouse model. These effects are mediated, at least in part, by the CK2α'-dependent phosphorylation of α-syn serine 129 in the striatum of HD mice, a post-translational modification associated with synucleinopathy and PD. Our study highlights a potential convergent mechanism of neurodegeneration between HD and PD and suggests targeting CK2α' as a therapeutic strategy to ameliorate neuroinflammation and synaptic dysfunction in HD and perhaps other neurodegenerative diseases.

Introduction

Huntington's disease (HD) is a neurodegenerative disorder that manifests with progressive motor, cognitive, and psychiatric deficits for which there is no cure. HD is caused by a poly-glutamine (polyQ) expansion in exon 1 of the Huntingtin (*HTT*) gene. This mutation results in progressive misfolding and aggregation of mutant HTT protein (mtHTT) and preferentially affects GABAergic medium spiny neurons (MSNs) in the striatum (1-3). Transcriptional perturbations in synaptic genes and neuroinflammation are key processes that precede MSN death and motor symptom onset (4). However, our understanding of the interplay between these processes, mtHTT aggregation, and their contribution to MSN susceptibility in HD is still incomplete.

Protein kinase CK2 is at the crossroads between neuroinflammation, protein aggregation, and synaptic activity, and has recently emerged as a potential therapeutic target of neurodegeneration (5, 6). CK2 is a highly conserved serine/threonine kinase composed of two regulatory beta (CK2β) subunits and two catalytic subunits, alpha (CK2α) and alpha prime (CK2α') (7, 8). The two catalytic subunits share high structural homology, but they differ in their tissue distribution and their ability to phosphorylate different substrates (9, 10). Our previous work showed that CK2α', but not CK2α, is induced in HD MSNs and is responsible for the phosphorylation and degradation of the heat shock transcription factor HSF1, the master regulator of chaperones and protein quality control systems (11, 12). CK2α'-dependent degradation of HSF1 contributes to chaperone dysregulation and HTT aggregation in cells and mouse models of HD (11). However, other studies conducted *in vitro* have suggested a protective role of CK2 in HD (13, 14), imposing the necessity to clarify the specific involvement of CK2α' in HD pathogenesis and its potential as a therapeutic target in HD.

CK2 is involved in the phosphorylation and aggregation of HTT (11, 14), as well as the phosphorylation and aggregation of other pathological proteins like microtubule associated protein tau (MAPT) and alpha-synuclein (α-syn), proteins involved in Alzheimer's (AD) and Parkinson's disease (PD) (15-17). Tau and α-syn contribute to the activation of neuroinflammatory processes, transcriptional dysregulation, and synaptic deficits in AD and PD [18, 19].These pathophysiological alterations are also observed in HD as well as the association of tau and α-syn in HD pathology (20, 21). Specific tau modifications and cleavage products associated with cognitive decline in AD were found in the brains of HD patients (21, 22), while increased levels of α-syn were observed in the plasma of patients with HD (23, 24). α-syn colocalized with mtHTT aggregates in the brains of R6/1 HD mice, and its deletion resulted in amelioration of motor deficits (20, 25). However, the mechanisms by which these proteins are altered in HD and the extent to which they contribute to HD pathophysiology is still unknown.

In this study, we characterized the role of CK2α' in HD *in vivo* by using the heterozygous zQ175 HD mouse model that lacks one allele of CK2α'. We showed that CK2α' haploinsufficiency decreased the levels of pro-inflammatory cytokines and improved astrocyte health, restored synaptic gene expression and excitatory synapse function, and improved motor behavior in zQ175 mice. These neuropathological and phenotypic changes correlated with alterations in α-syn serine 129 phosphorylation

(pS129-α-syn) in the striatum, a post-translational modification involved in α-synucleinopathy, establishing a novel connection between CK2α' function and synucleinopathy in HD. Collectively, our data demonstrated that CK2α' plays a negative role in HD and indicates the therapeutic potential of modulating CK2α' to achieve enhanced neuronal function and neuroprotection.

Results

Increased CK2α' levels in the striatum of zQ175 mice parallel progressive HTT aggregation and NeuN depletion

Increased CK2 activity has been associated with detrimental effects in protein homeostasis and neuroinflammation in different neurodegenerative diseases, but its role in HD is still controversial (11, 13, 14). To determine whether CK2α' plays a negative role during HD pathogenesis, we first evaluated the relationship between HTT aggregation, neuronal loss, and CK2α' levels in the striatum over time for the heterozygous zQ175 mouse model at 3 (pre-symptomatic), 6 (early symptomatic), 12 (symptomatic), and 22 months (late-stage disease) of age (26, 27). We observed an age-dependent increase of HTT aggregates ($EM48^+$ puncta) and a decreased number of $NeuN^+$ neurons (pan-neuronal marker) in the striatum of zQ175 mice (**Fig. 1A-D, S1A**). We confirmed that the depletion of $NeuN^+$ cells correlated with decreased $Ctip2^+$ neurons (MSN marker) (28)(**Fig. S1B, C**). However, we did not observe a significant difference in the total number of neurons, measured by cresyl violet (**Fig. S1D-F**), or in striatum volume (**Fig. S1G, H**), suggesting that changes in NeuN and Ctip2 reactivity may reflect transcriptional dysregulation and/or neuronal dysfunction rather than neuronal loss.

The levels of CK2α' increased over time in zQ175 mice in the striatum but not in the cortex (**Fig. 1E-G**), coinciding with HTT aggregation and preceding NeuN depletion. Regression analysis demonstrated that CK2α' levels had a significant positive relationship with HTT aggregation (Pearson $r(22)=0.87$, p value<0.001) (**Fig. 1H**) and a significant negative relationship with the number of $NeuN^+$ cells (Pearson $r(22)=-0.78$, p value<0.001) (**Fig. 1I**).

CK2α' haploinsufficiency reduced production of inflammatory cytokines in zQ175

CK2 regulates signaling pathways involved in inflammation (29). Inhibition of CK2 has previously shown to deplete pro-inflammatory cytokines such as IL-6 (6). IL-6 and other cytokines are increased in HD and are often used as a marker of disease progression (30). To determine whether the expression of CK2α' is directly related to neuronal-mediated inflammation in HD, we first analyzed the levels of IL-6 in the striatal-derived mouse cells ST*Hdh*$^{Q7/Q7}$ (control) and ST*Hdh*$^{Q111/Q111}$ (HD cells) (**Fig. 2A**). RT-qPCR analysis showed an upregulation of CK2α' in HD cells which paralleled an upregulation

159 of IL-6. CK2α' knock-down in HD cells reduced mRNA levels of IL-6 when compared to
160 non-targeting siRNA (scramble) (**Fig. 2B**).

161 To further explore the role of CK2α' in modulating inflammation in HD, we used the
162 zQ175 mouse model lacking one allele of CK2α' (zQ175:CK2α'$^{(+/-)}$) (**Fig. 2C, D**) which
163 has previously shown reduced HTT aggregation [11]. We analyzed the levels of 40
164 different cytokines and chemokines in the striatum of 12-14 month old mice (**Fig. 2E,**
165 **S2A-C**) and found seven cytokines (IFN-γ, IL-1α, IL-6, IL-7, IL-16, IL-17, IL-23, and
166 TNF-α) were decreased in zQ175:CK2α'$^{(+/-)}$ compared to zQ175 (**Fig. 2F**). This
167 suggests CK2α' contributes to the characteristic inflammatory profile of HD.

168 Inflammatory cytokines can be produced by both neurons and glial cells. Microglia are
169 pivotal regulators of CNS inflammatory processes and their activation has been
170 reported in numerous HD mouse models and in patients with HD (31-33). We evaluated
171 the levels of the microglial marker Iba1 (Ionized calcium binding adaptor molecule 1) by
172 immunoblotting (IB) and immunofluorescence (IF) in striatum extracts at 12-14 months
173 (**Fig. 2G, H, S2D-F**). Total Iba1 levels were significantly increased in zQ175 and
174 zQ175:CK2α'$^{(+/-)}$ mice compared to WT, but no significant differences were observed
175 between zQ175 and zQ175:CK2α'$^{(+/-)}$ mice. In addition, no changes were observed in
176 the number or area size of Iba1^{+} cells across all genotypes (**Fig. S2D-F**) and no
177 expression of IL-6 was seen in Iba1^{+} cells (**Fig. S3**), indicating that CK2α'-mediated
178 changes of pro-inflammatory cytokine levels may not be attributed to changes in
179 microglia. We then assessed whether astrocytes could contribute to inducing cytokines
180 in HD by co-staining IL-6 with different astrocyte markers (S100b, S100 Calcium
181 Binding Protein B; GFAP, Glial fibrillary acidic protein; and GS, glutamine synthetase)
182 (**Fig. S3**). Besides Ctip2, only GS^{+} astrocytes showed IL-6 immunoreactivity in zQ175
183 mice.

184

185 **CK2α' contributes to astrocyte pathology in HD**

186 Increases in the number of astrocytes and astrocytic dysfunction are reported in several
187 neurodegenerative diseases(34), including HD (35). As such, we tested whether the
188 changes in cytokine levels due to CK2α' haploinsufficiency were related to changes in
189 GS^{+} astrocytes during HD pathogenesis. We observed a progressive increase in the
190 number of GS^{+} astrocytes in the striatum of zQ175 mice compared to WT, and a
191 decrease in zQ175:CK2α'$^{(+/-)}$ mice (**Fig. 3A, B**). To confirm the changes observed in
192 astrocyte number in brain slices, we performed proton magnetic resonance
193 spectroscopy (^{1}H-MRS) *in vivo* at 22 months and measured the concentration of the
194 astroglia marker *myo*-inositol (Ins) (36, 37) and 14 additional brain metabolites (**Fig. 3C,**
195 **D, S4A, B**). The concentration of different neuronal metabolites including N-
196 acetylaspartate (NAA) and glutamate, which are dysregulated in HD (26, 38, 39), did not
197 differ between zQ175 and zQ175:CK2α'$^{(+/-)}$ mice (**Fig. S4A, B**). However, the levels of
198 *myo*-inositol (Ins) showed a significant reduction in zQ175:CK2α'$^{(+/-)}$ compared to zQ175
199 mice (**Fig. 3D**).

Cytokines like IL-1α, TNF-α, and complement component 1q (C1q) can induce the accumulation of the complement component C3d protein, a protein involved in innate immunity, altering astrocyte function and promoting astrocyte-dependent cytotoxicity during aging and neurodegeneration (40, 41). Increased depositions of C3d have been observed in the striatum of patients with HD and are considered a marker of astrocyte pathology (40, 42, 43). Since depletion of CK2α' decreased IL-1α and TNF-α levels, we evaluated the levels of C3d by IF and observed a significant age-dependent increase in the intensity of C3d in zQ175 mice compared to WT mice which was lower in zQ175:CK2α'$^{(+/-)}$ mice (**Fig. 3E, F**). C3d is expressed by different striatal components other than astrocytes [42] so we determined the fraction of GS^{+} astrocytes that showed C3d depositions (GS^{+}C3d^{+}) (**Fig. 3E, E', G**). The percentage of GS^{+}C3d^{+} astrocytes showed an age-dependent increase for all genotypes. The levels of C3d progressively increased in zQ175 mice (**Fig. 3G**), coinciding with the timing of CK2α' accumulation in MSNs (**Fig. 1C**). In contrast, zQ175:CK2α'$^{(+/-)}$ showed a significant reduction in GS^{+}C3d^{+} astrocytes compared to zQ175 mice at 12 and 22 months and no significant differences compared to WT mice (**Fig. 3G**), suggesting that neuronal accumulation of CK2α' contributes to astrocyte pathology in HD.

Depletion of CK2α' improves neuronal function and motor behavior

Astrocyte pathology contributes to progressive loss of striatal excitatory synaptic transmission and behavioral deficits associated with HD [44, 45]. This is supported by studies where conditional mutant HTT knock-out in astrocytes improved astrocyte function and restored both synaptic protein expression and MSN excitability in the BACHD mouse model (46). We assessed the impact of CK2α' depletion in AMPA-mediated excitatory transmission by conducting whole-cell patch clamp recordings from acute dorsolateral striatum coronal slices at 12 months (**Fig. 4A**). MSNs from all genotypes showed similar profiles in the analysis of basal synaptic transmission, including input/output curves, paired-pulse facilitation, and synaptic fatigue (**Fig. 4B-D**). We observed a trend towards increased normalized excitatory postsynaptic currents (EPSCs) in zQ175:CK2α'$^{(+/-)}$ mice compared to the other two genotypes, but the data did not reach statistical significance (**Fig. 4D**). Spontaneous neurotransmitter release and synaptic activity via miniature EPSC (mEPSC) recordings showed that mEPSC amplitude, reflecting postsynaptic AMPA receptor function, was comparable among the 3 genotypes (**Fig. 4E**). However, mEPSC frequency, which reflects the probability of neurotransmitter release from presynaptic vesicles and also correlates with the number of synapses, was reduced in zQ175 mice (**Fig. 4F, G**), as previously reported (47), and rescued in zQ175:CK2α'$^{(+/-)}$. CK2α' haploinsufficiency did not alter the number of MSNs (Ctip2^{+} cells) or the mRNA levels of the MSN markers (Drd1 and Drd2), but increased the levels of synaptic proteins like the scaffold protein Dlg4 (PSD-95) and Ppp1rb1 (dopamine- and cAMP-regulated neuronal phosphoprotein DARPP-32), a key regulator of the electrophysiological responses in striatal neurons (48, 49)(**Fig. S5A-C**). These data supported that astrocyte health can influence neuronal synaptic protein levels and excitability.

243 Glutamatergic synaptic transmission is often related to motor and cognitive function in
244 HD mouse models (45, 49). We conducted a series of motor tests including accelerating
245 rotarod and beam walk in WT, zQ175, and zQ175:CK2α'$^{(+/-)}$ mice at 3, 6, and 12 months
246 (**Fig. 5**). We also conducted cylinder and open field assessments on a different cohort
247 at 12 months comparing zQ175 and zQ175:CK2α'$^{(+/-)}$ (**Fig. S6**). We did not observe
248 significant differences between WT and zQ175 or between zQ175 and zQ175:CK2α'$^{(+/-)}$
249 at any tested age in the accelerating rotarod test (**Fig. 5A)**, open field, or cylinder test
250 (**Fig. S6**). However, when we evaluated fine motor coordination and whole body
251 balance in the beam test, we observed a significant increase in foot slips of zQ175 mice
252 compared to WT at 3 months, but only with the most challenging beam (small round),
253 indicating early subtle motor deficits (**Fig. 5B)**. At 12 months, zQ175 mice showed
254 increased foot slips in both the small round and small square beams compared to WT,
255 highlighting a worsening motor deficit. zQ175:CK2α'$^{(+/-)}$ mice showed a significant
256 reduction in foot slips compared to zQ175 mice at all tested ages and no significant
257 differences compared to WT.

258 We also performed tests to evaluate associative learning (fear conditioning), spatial
259 learning and memory (Barnes maze, BM), cognitive flexibility (BM reversal), and spatial
260 working memory (Y radial arm maze) by comparing zQ175 and zQ175:CK2α'$^{(+/-)}$ mice at
261 12 months of age, but no significant differences were observed between the two groups
262 (**Fig. S7**). This observation suggests that the positive effects of CK2α' depletion on
263 motor behavior may not additionally translate to improved cognitive functions.

264

265 **CK2α' depletion rescued gene expression of synaptic genes connected to alpha-**
266 **synuclein**

267 To elucidate the mechanism by which CK2α' contributes to HD, we investigated which
268 molecular pathways associated with HD could be specifically affected by CK2α'
269 haploinsufficiency. RNA-seq in the striatum of WT, zQ175, CK2α'$^{(+/-)}$, and
270 zQ175:CK2α'$^{(+/-)}$ mice at 12-14 months, followed by Weighted Gene Co-Expression
271 Network Analysis (WGCNA), revealed that the mouse transcriptome could be clustered
272 into 20 gene co-expression modules given the sample phenotypes (**Fig. S8, Table S1**).
273 Out of the 20 modules, 9 modules showed a significant difference in eigengene
274 expression between zQ175 and WT mice in a Kruskal-Wallis test (p value < 0.05) (**Fig.**
275 **S9A, Table S2**). Further evaluation of those 9 modules revealed 2 modules
276 (Greenyellow: 255 genes, and Red: 639 genes) were also significantly different between
277 zQ175 and zQ175:CK2α'$^{(+/-)}$ mice (p value < 0.05) (**Fig. 6A, Table S2**). Plots of module
278 eigengene expression confirmed that Greenyellow (**Fig. 6B)** and Red modules (**Fig. S8**)
279 were more consistent in the expression contrast between zQ175 mice and the rest of
280 the genotypes. Cook's distance (DESeq2) analyses revealed that these differences
281 were not due to the presence of outliers in our data set (**Fig. S9B**). Since the
282 Greenyellow module demonstrated a higher significance over the Red module (**Fig.**
283 **6A)**, we decided to focus our analyses on the Greenyellow module. Ingenuity pathway
284 analysis (IPA) indicated that the five most significant canonical pathways in the
285 Greenyellow module were synaptogenesis signaling pathways (p-value 1.68E-06),

286 Ephrin A signaling (p-value 7.84E-05), glutamate receptor signaling (p-value 1.98E-04),
287 axonal guidance signaling (p-value 7.13E-04), and G-protein coupled receptor (GPCR)
288 signaling (p-value 1.14E-03) (**Fig. 6C, Fig. S9C**), all of which have been previously
289 implicated in HD pathogenesis [(50)]. Additional Gene Ontology (GO) annotation of cellular
290 components indicated that Greenyellow genes are significantly enriched in synaptic
291 components (**Fig. 6D**).

292 Connectivity analyses (showing only 15% of the most highly connected members of the
293 Greenyellow module) (**Fig. 6E**) revealed that the two most connected genes within the
294 hub were Slit1 (Slit Guidance Ligand 1), associated with "poor" behavior and a worse
295 prognosis in the R6/1 mouse mode (51), and Ncald (Neurocalcin delta), which regulates
296 multiple endocytosis-dependent neuronal functions and is situated on a locus that has
297 been associated with earlier clinical onset of HD [(52, 53)]. To better understand which
298 specific genes were more impacted in their expression by CK2α' depletion, we
299 examined the Differential Gene Expression (DGE) between control mice (WT and
300 CK2α'$^{(+/-)}$) and HD mice (zQ175 and zQ175:CK2α'$^{(+/-)}$) (**Table S3**). The DGE between
301 WT and zQ175 mice confirmed a large transcriptional dysregulation (n=885 genes,
302 Q<0.1) (**Fig. S9D, E Table S3**), as previously reported [(50)]. Interestingly, the DGE
303 between zQ175:CK2α'$^{(+/-)}$ and WT mice only reported 123 genes, in contrast to the 885
304 genes between zQ175 and WT (**Fig. S9F, G**). Since our sample distribution was not
305 equally sex balanced, we then used R package variance Partition and confirmed that
306 these expression changes were driven only by 'genotype' and not by 'sex' (**Fig. S9H**).

307 CK2α' depletion decreased inflammation and improved astrocyte health. Therefore, we
308 searched for microglial and astrocytic inflammatory RNA signatures in our data set (40).
309 As Castro-Diaz et al., showed (43), we did not observe significant changes in the
310 expression of these gene signatures even when comparing WT and zQ175 mice (**Fig.
311 S10A, B, Table S4, S5**). The disconnection between changes in protein levels of
312 inflammatory cytokines and the absence of transcriptional alterations in those genes
313 could be explained by post-translational events potentially regulated by CK2α'.
314 However, we recapitulate some transcriptional changes for genes of the HD-associated
315 astrocyte molecular signature in the zQ175 mice (43, 54), indicative of astrocytic
316 dysfunction (**Fig. S10C**). Notably, these changes were not observed when comparing
317 zQ175:CK2α'$^{(+/-)}$ and WT mice.

318 The DGEs analyzed between zQ175 and zQ175:CK2α'$^{(+/-)}$ mice revealed 39 specific
319 and significant genes (FDR<0.1) (**Fig. 6F, Table S6**), including Csnk2a2 (CK2α' gene)
320 as a positive control. Three genes (Ncald, Nrp2, and Slc30a3) were also among the
321 15% most highly connected members of the Greenyellow module (**Fig. 6E**). At least
322 40% of the DGEs (n=16) were related to synaptic functions (**Fig. 6F, Table S6**). We
323 performed an IPA on the 39 genes to query for biological meaning and found that the
324 most significant canonical pathway was for glutamate receptor signaling (p-value 2.09E-
325 03) (**Fig. 6A**). These pieces of data confirm the contribution of CK2α' to the
326 dysregulation of genes related to excitatory synaptic transmission in HD.

327 When looking at the most significant upstream regulators identified by IPA of both the
328 Greenyellow module and the 39 gene set identified by DGE, we found SNCA (alpha-

329 synuclein) (p-value 9.10E-11 and 1.03E-07, respectively). α-syn is a neuronal protein
330 that regulates multiple processes, including synaptic vesicle trafficking and
331 neurotransmitter release and transcription, and is associated with onset and
332 progression of Parkinson's disease (55, 56). α-syn was also shown to exert a toxic
333 effect in R6/1 mice, but its mechanism of action has remained unknown(20, 25). IPA
334 connected α-syn with some of the most differentially dysregulated genes in the set of 39
335 genes associated to synaptic functions including Ttr (Transthyretin), Grm2 (Glutamate
336 Metabotropic Receptor 2), Slc17a7 (Solute Carrier Family 17 Member 7; alias VGlut1),
337 C1ql3 (Complement Component 1, Q Subcomponent-Like), Cckbr (cholecystokinin B
338 receptor), Nrp2 (Neuropilin 2), and the transcription factors Tbr1 (T-Box Brain
339 Transcription Factor 1) and Nr4a2 (Nuclear Receptor Subfamily 4 Group A Member 2;
340 alias Nurr1) (**Fig. 6G, F)**.

341 To determine the extent to which α-syn participates in the regulation of genes identified
342 in our IPA analyses (**Fig. 6G**), we used R6/1:SNCA^{KO} mice (**Fig. S11**), previously
343 shown to improve in motor behavior compared to R6/1 mice [20]. RT-qPCR showed
344 significant expression changes for SNCA, Nrp2, Cckbr, and Ttr between WT and R6/1
345 mice. Lack of SNCA significantly decreased the expression of Slc30a3 and Grm2, and
346 showed a trend toward decreased expression for Ttr and Cckbr in R6/1:SNCA^{KO}
347 compared to R6/1 mice. In addition, nearly all tested genes decreased their expression
348 when comparing R6/1:SNCA^{KO} to WT:SNCA^{KO}. Altogether, this data suggested that
349 transcriptional dysregulation of some synaptic genes in HD could be mediated by α-syn
350 dysfunction. Although some gene expression changes differed between R6/1 and
351 zQ175 mice, the effects mediated by SNCA^{KO} demonstrated a role of α-syn in the
352 regulation of the genes identified in our IPA analyses in HD.

353

354 **Striatal synucleinopathy is found in zQ175 mice and is reduced by CK2α'**
355 **depletion**

356 We next explored whether CK2α' was involved in the regulation of α-syn in HD. We
357 observed that the total amount of α-syn was similar between WT and zQ175 (**Fig. 7A-C**)
358 mice. zQ175:CK2α'$^{(+/-)}$ mice showed a trend towards increased α-syn, but did not reach
359 statistical significance (**Fig. 7B, C**). Nuclear and cytoplasm fractionation confirmed the
360 presence of α-syn in nuclear fractions from striatum samples (55, 57), and showed a
361 modest but significant increase in nuclear α-syn in zQ175 mice (**Fig. 7D, E**). IF analyses
362 for α-syn and HTT (EM48) also confirmed the colocalization between these two
363 proteins, as previously shown in R6/1 mice (20)(**Fig. 7F, G**). To determine if there was a
364 difference in the number and distribution of co-localized α-syn/HTT, we first analyzed
365 the number of EM48^{+} puncta in both the nucleus and cytoplasm between zQ175 and
366 zQ175:CK2α'$^{(+/-)}$ mice. Cytoplasmic HTT aggregates were reduced in zQ175:CK2α'$^{(+/-)}$
367 compared to zQ175 mice, consistent with previous studies (11), although no significant
368 differences were observed in the number of nuclear HTT aggregates (**Fig. 7H, I**).
369 Despite the decrease in cytoplasmic HTT aggregates in zQ175:CK2α'$^{(+/-)}$ mice, no
370 significant differences were observed in the number of nuclear and/or cytoplasmic α-
371 syn/HTT colocalized puncta between zQ175 and zQ175:CK2α'$^{(+/-)}$ mice (**Fig. 7J**).

372 We then evaluated whether pS129-α-syn, a marker of synucleinopathy (58, 59), was
373 altered in HD and whether CK2α' could influence its levels. We observed that the levels
374 of pS129-α-syn increased in the striatum of zQ175 mice at 12 months compared to WT
375 (tested with 3 different pS129-α-syn antibodies: 81A, EP1536Y and D1R1R), and in the
376 striatum of patients with HD (**Fig. 8A-E, Fig. S12A**), indicating signs of synucleinopathy.
377 The levels of pS129-α-syn were significantly reduced in zQ175:CK2α'$^{(+/-)}$ mice
378 compared to zQ175, while no significant differences were observed with WT mice (**Fig.**
379 **8D, E, Fig. S12A-C**). pS129-α-syn was detected in both the cytoplasm and the nucleus
380 of zQ175 striatal cells, while no nuclear presence was detected in zQ175:CK2α'$^{(+/-)}$ mice
381 (**Fig. 8F, G**). In addition, we observed that pS129-α-syn colocalized with both
382 cytoplasmic and nuclear HTT puncta in zQ175 mice, while only cytoplasmic
383 colocalization was observed in zQ175:CK2α'$^{(+/-)}$ mice (**Fig. 8F, G, Suppl. Video 1**).

384

385 **Discussion**

386 Increased protein kinase CK2 activity has been associated with detrimental effects in
387 protein homeostasis and neuroinflammation in different neurodegenerative diseases,
388 including AD and PD (5). However, the role of CK2 in HD remained unclear. This study
389 demonstrated the adverse effects of the catalytic subunit CK2α' on neuroinflammation,
390 protein aggregation, neuronal function, and motor behavior in the zQ175 HD mouse
391 model and consolidated the important contribution of CK2α' to HD pathogenesis. We
392 also found this contribution is mediated, at least in part, by the ability of CK2α' to
393 phosphorylate α-syn and induce striatal synucleinopathy and synaptic gene
394 dysregulation (**Fig. 8H**).

395 We previously showed that CK2α' levels were induced in the striatum of patients with
396 HD, in MSN-like human iPSCs derived from patients with HD, and in zQ175 mouse
397 MSNs (11). CK2α' upregulation was associated with HD pathogenesis since CK2α'
398 genetic knockdown in different HD cell models resulted in decreased HTT aggregation
399 and increased cell viability(11). However, other studies using CK2 inhibitors suggested
400 CK2 induction as a protective mechanism in HD (13, 14). These conflicting reports
401 could be explained by the poor selectivity and high toxicity of previously used CK2
402 inhibitors (60). Our study demonstrated that reducing levels of CK2α' by removing one
403 allele of the Csnk2a2 (CK2α') gene in the zQ175 heterozygous HD mouse model
404 (zQ175:CK2α'$^{(+/-)}$) had significant and long-term benefits in several HD-related
405 phenotypes. CK2α' depletion significantly altered the production of several pro-
406 inflammatory cytokines in the striatum of symptomatic zQ175 mice. The benefits of
407 reducing neuroinflammation in HD have been shown in R6/2 mice intracranially injected
408 with a TNF-α inhibitor, which resulted in a significant increase in neuronal density and
409 improved motor function [61]. We obtained similar results when reducing the expression
410 of CK2α', suggesting CK2α' as a potential upstream regulator of neuroinflammation in
411 HD.

412 Neuroinflammation is a coordinated response to brain toxicity, involving the activation of
413 microglia and astrocytes. Increased reactive microglia were reported in numerous HD

414 mouse models [31, 33, 62] and in pre-symptomatic patients with HD (31, 32), and are often
415 associated with increased pro-inflammatory cytokines (4). However, our microglia
416 analyses failed to show robust microgliosis in zQ175 mice, consistent with previous
417 studies (43), and did not indicate microglia as a relevant cell type responsible for the
418 inflammatory profile observed in zQ175 or for the changes mediated by CK2α'
419 depletion. On the contrary, we observed increased astrogliosis in zQ175 mice,
420 manifested by an increased number of astrocytes and astrocytic pathology, which
421 decreased in zQ175:CK2α'$^{(+/-)}$. Although it is unknown how CK2α' influences astrocyte
422 proliferation, it has been shown that specific cytokines like TNF-α and IL-6 have a
423 proliferative effect on astrocytes (63) and therefore, CK2α'-mediated changes in these
424 cytokines could be responsible for these phenotypes in HD mice.

425 Accumulation of C3 and the C3 cleaved product, C3d, in HD astrocytes is canonically
426 considered a marker of astrocytic pathology associated with neuroinflammation (40, 42,
427 43). Liddelow et al., reported that astrocytes react to the presence of specific cytokines,
428 such as IL-1α, TNF-α, and C1q, by changing their transcriptional program and adopting
429 a neurotoxic phenotype (A1), which is also characterized by the accumulation of C3d
430 (40). Transcriptomic studies in purified HD astrocytes [43] and our own RNA-seq data
431 have failed to identify transcriptional changes characteristic of A1 astrocytes, but
432 instead revealed a transcriptional signature related to astrocytic dysfunction that is
433 associated with the activation of C3d. In AD, expression of C3d in astrocytes is induced
434 by neuroinflammatory processes triggered by amyloid-beta, and its activation
435 contributes to protein aggregation and cell death(64). CK2 phosphorylates C3 and
436 modulates its cleavage and activation(65). Therefore, CK2α' levels, as well as CK2α'-
437 mediated neuroinflammation, could influence C3d accumulation in astrocytes and
438 astrocytic pathology.

439 Increased pro-inflammatory cytokines can alter synaptic strength as well as
440 glutamatergic transmission and are also associated with structural and functional
441 disruption of synaptic compartments (66). Similarly, astrocyte dysfunction in HD
442 contributes to reduced striatal glutamatergic transmission and spine density, ultimately
443 decreasing MSN excitability(35, 46). We showed that CK2α'-dependent decrease of
444 inflammatory cytokines and astrogliosis correlated with increased expression of synaptic
445 proteins (PSD-95 and Darpp-32) and improved AMPA-mediated synaptic transmission.
446 Similarly, conditional deletion of mtHTT in astrocytes of BACHD mice rescued the
447 expression of synaptic proteins and synaptic activity in the striatum and improved
448 astrocyte health(46). However, whether decreased astrocytic pathology contributes to
449 improved neuronal activity in zQ175:CK2α'$^{(+/-)}$ mice is yet to be determined.

450 In contrast to CK2α, which is an essential protein with hundreds of targets, CK2α' has
451 very few identified substrates (9, 67). We previously showed the stress protective
452 transcription factor HSF1 as a substrate of CK2α' (11). HSF1 is the master regulator of
453 protein homeostasis in mammalian cells and has also been linked to the regulation of
454 anti-inflammatory and synaptic processes (12). CK2α' phosphorylates HSF1, signaling
455 HSF1 for proteasomal degradation and influencing chaperone expression and HTT
456 aggregation in cells and in HD mice (11). Our RNA-seq analysis validated the increased
457 expression of chaperones like Hsp70 and Hsp25 in the zQ175:CK2α'$^{(+/-)}$ mice,

458 consistent with previous findings (11). However, WGCNA and DGE did not reveal global
459 changes in specific transcriptional pathways associated with protein quality control
460 networks between zQ175 and zQ175:CK2α'$^{(+/-)}$, but instead showed two different
461 modules (Greenyellow and Red) primarily corresponding to signaling pathways related
462 to synaptogenesis and glutamate receptor signaling. SNCA (α-syn) was indicated by
463 IPA as one of the top putative upstream regulators of the CK2α'-mediated
464 transcriptional changes observed by WGCNA and DGE analyses. Although α-syn is not
465 a transcription factor, several reports have shown α-syn has the ability to modulate the
466 expression of transcription factors like Nurr1, which is involved in the regulation of
467 inflammation and is differentially expressed between zQ175 and zQ175:CK2α'$^{(+/-)}$ mice
468 (55, 56). α-syn aggregation is thought to be a key process in PD and other
469 synucleinopathies and is promoted by the presence of high levels of α-syn
470 phosphorylation and ubiquitylation (59). In particular, pS129-α-syn phosphorylation
471 regulates neurotransmitter uptake, notably dopamine as well as glutamate release,
472 thereby playing an important role at synaptic terminals and modulating synaptic
473 plasticity (59, 68).

474 The specific contribution of α-syn dysregulation in HD has yet to be determined. It is
475 known that α-syn participates in HD pathogenesis because α-syn KO mice have
476 demonstrated decreased mtHTT aggregation and attenuated body weight loss and
477 motor symptoms in R6/1 mice (20, 25). Interestingly, aggregation of α-syn and
478 consequent synucleinopathy in PD has been linked to the activation of CK2 and CK2-
479 dependent phosphorylation, although it is unknown which CK2 subunit participates in
480 this process (69). α-syn has also been shown to influence cytokine production (70).
481 Therefore, it is reasonable to hypothesize that CK2α' could contribute to HD by
482 increasing HTT aggregation via dysregulation of protein quality control mechanisms
483 and/or increasing α-syn phosphorylation. Here, we showed increased pS129-α-syn in
484 the striatum of symptomatic HD mice and patients with HD as well as an increased
485 localization of this phosphorylated form in the nucleus. Furthermore, we demonstrated
486 that CK2α' is involved in this process. Decreased phosphorylation and the accumulation
487 of pS129-α-syn in the nucleus could be responsible for the rescue of α-syn-associated
488 transcriptional alterations and the improvement of synaptic function, cytokine
489 expression, and astrocytic pathology seen in zQ175:CK2α'$^{(+/-)}$ mice. Overall, these
490 results provide strong evidence for CK2α' playing an important role in many aspects of
491 HD pathogenesis, supporting its potential as a therapeutic target in HD. Further
492 experiments will be necessary to decipher the mechanism by which CK2α'-mediated α-
493 synucleinopathy contributes to HD and to tease apart the differential contribution of HTT
494 aggregation and α-syn pathology to the symptomatology, onset, and progression of HD.

495

496 **Materials and Methods**

497 **Cell lines**

498 Mammalian cell lines used in this study were the mouse-derived striatal cells STHdh^{Q7}
499 and STHdh^{Q111} (Coriell Cell Repositories). Cell lines were authenticated by

500 immunoblotting for the detection of mutant HTT protein. Cells were grown at 33ºC in
501 Dulbecco's modified Eagle's medium (DMEM, Genesee) supplemented with 10% fetal
502 bovine serum (FBS), 100 U ml^{-1} penicillin/streptomycin and 100 ug ml^{-1} G418 (Gibco),
503 as previously described (11).

504

505 **Mouse strains**

506 All reported data abides to the ARRIVE guidelines for reporting animal research. For
507 this study we used a full-length knock-in mouse model of HD known as zQ175 on the
508 C57BL/6J background (B6J.zQ175 KI mice (Stock No. 027410)), which harbors a
509 chimeric human/mouse exon 1 carrying an expansion of ~188 CAG repeats and the
510 human poly-proline region (27). WT (C57BL/6) animals were used as controls. CK2α′
511 heterozygous mice ($CK2\alpha'^{(+/-)}$) on the 129/SvEv-C57BL/6J background (Taconic
512 Biosciences TF3062) were originally obtained from Dr. Seldin (Boston University) (71).
513 $CK2\alpha'^{(+/-)}$ were crossbred with WT and zQ175 for more than 10 generations prior to
514 selecting the founder animals of the study. All mice used have the C57BL/6J
515 background. All mice were housed under standard SPF conditions in a conventional
516 12:12 *light*/*dark* cycle. All experiments were conducted during the light cycle. Mice were
517 bred as previously described [11] to generate the following genotypes: WT ($CK2\alpha'^{(+/+)}$
518 $HTT^{(0/0)}$), $CK2\alpha'^{(+/-)}$ ($CK2\alpha'^{(+/-)}$ $HTT^{(0/0)}$), zQ175 ($CK2\alpha'^{(+/+)}$ $HTT^{(Tg/0)}$), zQ175;$CK2\alpha'^{(+/-)}$
519 ($CK2\alpha'^{(+/-)}$ $HTT^{(Tg/0)}$). Animals were analyzed at 3, 6, 12, and 22 months of age. We also
520 used samples from 5 month WT (mixed background CBA x C57BL/6), R6/1, $SNCA^{KO}$,
521 and R6/1$SNCA^{KO}$ obtained from Dr. Lucas. Sample size was set to a minimum of three
522 animals per genotype for every analysis. When possible, at least two females and two
523 males were used for each genotype and age. Littermates of the same sex were
524 randomly assigned to experimental groups. All animal care and sacrifice procedures
525 were approved by the University of Minnesota Institutional Animal Care and Use
526 Committee (IACUC) in compliance with the National Institutes of Health guidelines for
527 the care and use of laboratory animals under the approved animal protocol 2007-
528 38316A.

529

530 **siRNA transfection**

531 For CK2α' knock-down, ST*Hdh* cells were transfected with FlexiTube siRNA (5 nmol)
532 from Qiagen (Mm_Csnk2a2; SI00961051; SI00961058; SI00961065; SI00961072)
533 using DharmaFECT1 per manufacturer's guidelines. As a negative control, ON-
534 TARGETplus control Non-targeting pool siRNA (Dharmacon) was used. Cells were
535 collected 24 h after transfection for RNA extraction and RT-qPCR. All siRNAs have
536 been validated by RT-qPCR and immunoblotting for knockdown efficiency of the target
537 gene.

538

539 **RNA preparation and RT-qPCR**

540 RNA was extracted from STHdh cells and mouse striatal tissues by using the RNeasy
541 extraction kit (Qiagen) according to the manufacturer's instructions. cDNA for all

542 samples was prepared from 1 µg RNA using the Superscript First Strand Synthesis
543 System (Invitrogen) according to the manufacturer's instructions. SYBR green based
544 PCR was performed with SYBR mix (Roche). The primer sequences for target genes
545 were as follows: CK2α' forward: 5'- CGACTGATTGATTGGGGTCT-3' reverse: 5'-
546 AGAATGGCTCCTTTCGGAAT-3', IL-6 forward: 5'- AGTTGCCTTCTTGGGACT-3'
547 reverse: 5'-TCCACGATTTCCCAGAGAAC-3', PSD-95 (Dlg4) forward: 5'-
548 CCGACAAGTTTGGATCCTGT-3', reverse: 5'-ACGGATGAAGATGGCGATAG, Drd1
549 forward: 5'-AAGATGCCGAGGATGACAAC-3', reverse:5'-
550 CCCTCTCCAAAGCTGAGATG-3', Drd2 forward: 5'-TATGCCCTGGGTCGTCTATC-3',
551 reverse: 5'-AGGACAGGACCCAGACAATG-3', Darpp32(PPP1R1B) forward: 5'-
552 CCACCCAAAGTCGAAGAGAC-3', reverse: 5'-GCTAATGGTCTGCAGGTGCT-3',
553 GAPDH (used as an internal control gene) forward: 5'-AACTTTGGCATTGTGGAAGG-
554 3' reverse: 5'-ACACATTGGGGGTAGGAACA-3'. The qPCR amplification was
555 performed using the LightCycler 480 System (Roche). Each sample was tested in
556 triplicate and normalized to GAPDH levels. For analysis, the $2^{\Delta\Delta Ct}$ method was used to
557 calculate the relative fold gene expression of samples.
558

559 **Immunoblot analysis**

560 Sample preparation and immunoblotting condition were performed as previously
561 described (11). Striatum protein extracts from one hemisphere of mice were prepared in
562 cell lysis buffer (25 mM Tris pH 7.4, 150 mM NaCl, 1 mM EDTA, 1% Triton-X100 and
563 0.1% SDS). Extra SDS was added to the suspension to a final concentration of 2% (w
564 per v) and lysates heated at 95°C for 5 min to solubilize tissue. Total tissue homogenate
565 was then centrifuged at 12,000 r.p.m. for 10 min. Protein samples were separated on 4–
566 20% SDS Criterion TGX Stain-Free gels (BioRad) at 110 V. Proteins were transferred to
567 a nitrocellulose membrane (BioRad 0.2 µm) and blocked with 5% non-fat dry milk in
568 TBS containing 0.25% Tween-20 (TBST) for 1 h at room temperature. Primary
569 antibodies were anti-CK2α' (Rabbit, Novus NB100-379 and Proteintech 10606-1-AP,
570 both 1:1000), anti-Iba1 (Rabbit, FUJIFILM Wako 019-19741, 1:1000), α-syn (Mouse,
571 Biolegend 834303, 1:1000, clone 4D6), pS129-α-syn (Mouse, Millipore MABN826,
572 1:500, clone 81A and Rabbit, EP1536Y Abcam ab51253, 1:1000), GAPDH (Mouse,
573 Santacruz sc-365062, 1:10000). Quantitative analyses were performed using ImageJ
574 software and normalized to GAPDH controls.

575

576 **Immunohistochemistry**

577 Mice were anesthetized with Avertin (250 mg/kg Tribromoethanol) and perfused
578 intracardially with 25mM Tris-base, 135mM Nacl, 3mM KCl, pH 7.6 supplemented with
579 7.5 mM heparin. Brains were dissected, fixed with 4% PFA in TBS at 4°C for 4-5 days,
580 cryoprotected with 30% sucrose in TBS for 4-5 days and embedded in a 2:1 mixture of
581 30% sucrose in TBS:OCT (Tissue-Tek). Immunostaining was performed as previously
582 described (11). Fluorescent images acquired on an epi-fluorescent microscope (Echo
583 Revolve) or confocal microscope (Olympus FV1000). Primary antibodies used and

584 dilutions are as follows: α-syn (Mouse, Biolegend 834303, 1:1000), pS129-α-syn
585 (Mouse, Millipore MABN826, 1:500 and Rabbit, D1R1R Cell signaling technology
586 23076S, 1:200), CK2α' (Rabbit, Proteintech 10606-1-AP, 1:500), Ctip2 (Rat, Abcam
587 ab18465, 1:500), complement component C3d (Goat, R&D Systems AF2655,
588 1:200), Glial fibrillary acidic protein GFAP (Rabbit, Invitrogen PA1-10019, 1:500), S100
589 Calcium Binding Protein B S100b (Rabbit, Abcam ab41548, 1:500), glutamine
590 synthetase GS (Mouse, BD Biosciences 610517, 1:1000 and Rabbit, Abcam 49873,
591 1:500), HTT (Mouse, Millipore, clone mEM48 Mab5374, 1:100, and Rabbit, Abcam
592 ab109115, 1:500), Iba1 (Rabbit, FUJIFILM Wako 019-19741, 1:200), NeuN (Mouse,
593 Millipore MAB377, 1:1000), IL-6 (Mouse, Santa Cruz Bio sc-32296, 1:100). For cell
594 number (Ctip, GS, NeuN, Iba1, DAPI) the Cell counter plugin from ImageJ software was
595 used and normalized to the image area (300μm^2). EM48$^+$ aggregates were counted
596 using annotations in the Echo Revolve software and validated using the Puncta
597 Analyzer plugin in ImageJ. Number of pS129-α-syn/EM48 puncta was calculated using
598 the Puncta Analyzer plugin in ImageJ.

599

600 **Cytokine and chemokine array**

601 The Proteome Profiler Mouse Cytokine Array Panel (ARY006, R&D Systems) was used
602 to detect the levels of cytokine/chemokine of the mouse brain as per manufacturer's
603 instructions. Frozen striatum from 12 - 14 months was homogenized in PBS containing
604 Halt protease inhibitor cocktail and phosphatase inhibitors (Fisher Scientific) and 1%
605 triton X-100 (Sigma). Samples were stored at -80°C for 15 min, thawed and centrifuged
606 at 10,000 × g for 5 min to remove cell debris. A total of n=6 mice/genotype with a
607 female(F)/male(M) ratio (3F/3M WT, 5F/1M zQ175, and 4F/2M zQ175:CK2α'$^{(+/-)}$) were
608 analyzed. Samples were grouped in three different pools for each genotype: pools 1
609 and 2 contained three different mice per genotype, pool 3 contained a randomized
610 selection of 3 mice/genotype out the n=6 mice cohort. Similar numbers of male and
611 female mice were evaluated. Data was analyzed using ImageJ software and presented
612 as an average signal of three independent pool assays, calculating pairs of duplicate
613 spots corresponding to 40 different cytokines or chemokines.

614

615 **Nuclear/Cytoplasm fractionation**

616 Frozen striatum samples (~20 mg) were fractionated using the Minute™ Cytosolic and
617 Nuclear Extraction Kit for Frozen/Fresh tissues (Invent Biotechnologies INC, Cat NT-
618 032) as per Manufacturer's instructions.

619

620 **Cresyl Violet staining**

621 Coronal brain slices were mounted on Fisherbrand Superfrost Plus Microscope Slide
622 and dried at 37 ºC overnight. Dried sections were incubated with 0.2% Cresyl violet
623 acetate (Sigma #C5042) pH 3.7 for 8 minutes. Samples were then dehydrated in 80%,

95%, and 100% Ethanol solution for two minutes each followed by Xylene incubation. Slides were dried and mounted with permount (#SP15-500) and imaged on a Leica DM2500. Neurons were identified as round light blue cells and manually counted.

Electrophysiological analyses

Acute dorsolateral striatum coronal slices (350 µm thick) were obtained from approximately 12 months old mice using a vibratome, and processed as previously described (72). Researchers were blind to the mouse genotype. The brain was quickly removed after decapitation and placed in ice-cold artificial cerebrospinal fluid (ACSF). Slices were incubated for at least 1h before use in a chamber at room temperature (21–24 ºC) in ACSF containing (in mM): NaCl 124, KCl 2.69, KH_2PO_4 1.25, $MgSO_4$ 2, $NaHCO_3$ 26, $CaCl_2$ 2, ascorbic acid 0.4, and glucose 10, and continuously bubbled with carbogen (95% O_2 and 5% CO_2) (pH 7.4). Slices were then transferred to an immersion recording chamber and superfused at 2 mL/min with gassed ACSF at 30-32 ºC and visualized under an Olympus BX50WI microscope (Olympus Optical; Japan). To study excitatory postsynaptic currents (EPSCs) picrotoxin (50 µM) and CGP54626 (1 µM) were added to the solution to block the $GABA_A$ and $GABA_B$ receptors, respectively. Whole-cell electrophysiological recordings were obtained from medium spiny neurons (MSNs) using patch electrodes (3–10 MΩ) filled with an internal solution containing (in mM): $KMeSO_4$ 135, KCl 10, HEPES-K 10, NaCl 5, ATP-Mg 2.5, GTP-Na 0.3 (pH 7.3). Recordings were obtained with a PC-ONE amplifier (Dagan Instruments; Minneapolis, MN, USA). Membrane potentials were held at −70 mV. Signals were filtered at 1 kHz, acquired at a 10 kHz sampling rate, and fed to a Digidata 1440A digitizer (Molecular Devices; San Jose, CA, USA). pCLAMP 10.4 (Axon Instruments, Molecular Devices; San Jose, CA, USA) was used for stimulus generation, data display, data acquisition, and data storage. To record evoked EPSCs, theta capillaries filled with ACSF were used for bipolar stimulation and placed in the vicinity of the cell patched in the dorsolateral striatum. Input–output curves of EPSCs were made by increasing stimulus intensities from 0 to 100 µA. Paired-pulse facilitation was done by applying paired pulses (2 ms duration) with 25, 50, 75, 100, 200, 300, and 500 ms inter-pulse intervals. The paired-pulse ratio was calculated by dividing the amplitude of the second EPSC by the first (PPR=EPSC-2/EPSC-1). Synaptic fatigue was assessed by applying 30 consecutive stimuli in 15 ms intervals. For miniature EPSCs (mEPSCs) tetrodotoxin (TTX; 1 µM) was added to the solution.

Magnetic resonance imaging and spectroscopy

Animal Preparation for MR Scanning: Researchers were blinded to the genotype of the mice during testing. Animals were induced with 3% isoflurane in a 1:1 mixture of O_2:N_2O. Mice were secured in a custom-built mouse holder and physiological status was monitored (SA Instruments) and recorded. Anesthesia was maintained with 1.5-2% isoflurane to achieve a respiration rate of 70-100 breaths per minute. Body temperature

665 was maintained at 36-37ºC with a circulating warm water system and a heating fan
666 controlled by feedback received from a fiber-optic rectal thermometer. The scan session
667 was approximately 50 minutes for each animal. MR Protocol: All experiments were
668 performed on a 9.4T/31 cm scanner (Agilent), as described previously (73). See
669 **Supplementary Methods** for details.

670

671 **Measurement of striatal volume**

672 For volumetric analysis of striatum, coronal RARE images were used. The images had
673 an in-plane resolution of 0.125 mm x 0.125 mm and 1 mm slice thickness. All volumetric
674 quantifications were performed using ImageJ. The perimeter of the striatum was traced
675 using a polygon selection tool and the volume measurement was performed by running
676 Measure Stack plugin on ImageJ. All quantitative analyses were conducted blindly with
677 respect to mouse genotype.

678

679 **Behavioral assays**

680 Researchers at the Mouse Behavioral core at University of Minnesota were blind to the
681 genotypes of the mice during testing. Mice were transported from their colony room in
682 their home cages to the behavioral testing room, where they were allowed to acclimate
683 for at least one hour prior to the beginning of the experiment. See **Supplementary**
684 **Methods** for a complete description of all behavioral tests conducted in the study.

685 *Beam Walk*: The deficits of motor coordination were assessed by a beam walking test
686 which measures a mouse's ability to maintain balance while traversing a narrow beam
687 to reach a safe platform. For this, 19-mm (medium-round) or 10-mm (small-round)
688 diameter and 16-mm (medium-Square) or 10-mm (small-Square) width of 3 feet long
689 wood beams (made in house) were used and placed 19 inches above the test bench by
690 metal supports. Each mouse was placed on the beam at one end and allowed to walk to
691 the goal box. Foot slips were recorded manually when the hind paws slipped off the
692 beam. Testing included 3 training days with 4 consecutive trials. The performance was
693 measured by recording the time of traversing the beam and the number of paw faults or
694 slips from the beam. Maximum length of time per trial was 60 s; trials that exceeded 60
695 s (e.g. a mouse failed to cross the finish line within a minute) were recorded as 60 s.

696 *Rotarod*: It is a standard test of motor coordination and balance in rodents. Mice were
697 tested over 3 consecutive days. Each daily session included a single training trial of 15
698 min at 5 RPM on the rotarod apparatus (Ugo Basile). On day 3, the animals were tested
699 for 3 consecutive accelerating trials of 5 min with the rotarod speed changing from 5 to
700 50 RPM over 300 s, with an inter-trial interval of at least 15 min. The latency to fall from
701 the rod was recorded for each trial with mice remaining on the rod for more than 300 s
702 removed and scored at 300 s.

703

RNA-Seq Analyses

Gene expression analysis was carried out using the CHURP pipeline (HTTps://doi.org/10.1145/3332186.3333156) using n=5 mice/genotype for WT, zQ175, and zQ175:CK2α'$^{(+/-)}$ and n=3 mice for CK2α'$^{(+/-)}$, with a female (F)/male (M) ratio: 4F/1M WT, 1F/2M CK2α'$^{(+/-)}$, 2F/3M zQ175, 4F/1M zQ175:CK2α'$^{(+/-)}$. Read quality was assessed using FastQC (HTTp://www.bioinformatics.bbsrc.ac.uk/projects/fastqc). Raw reads were then trimmed to remove low quality 3' ends and adaptor contamination using Trimmomatic with the following parameter: ILLUMINACLIP:all_illumina_adapters.fa:4:15:7:2:true LEADING:3 TRAILING:3 SLIDINGWINDOW:4:15 MINLEN:18 (74). Processed reads were aligned to mouse reference genome GRCm38 via HiSat2 (PMID: 31375807) using default parameters. Post-alignment cleaning removed duplicated mapping, unmapped reads, and reads with MAPQ<60. Gene-level expressions were quantified using Subread (PMID: 24227677), and differential gene expression was determined with DESeq2 using default setting (PMID: 25516281). Genes with a q < 0.1 were considered significant. Outliers' identification was performed using Cook's distance (DESeq2), which is a measure of how much a single sample is influencing the fitted coefficients for a gene. Driver factors of gene expression variance (genotype and/or sex) were evaluated using R package variance Partition. Pathway and clustering analysis were completed with Ingenuity Pathway Analysis (Ingenuity Systems: RRID: SCR_008653) and gProfiler2 (PMID: 31066453). Data visualization was done using various R graphic packages, including ggplo2, ggraph, and DESeq2 visualization functions. The RNA-seq data set generated in this manuscript has been deposited at GEO (accession number GSE160586). Reviewer token "**gpqrigisbxgprqf".**

WGCNA Analysis

Genes with less than 10 counts in more than 90% of samples were removed from WGCNA analysis (75). The count-based gene expressions were first transformed using a variance stabilizing method via DESeq2 vst function. The WGCNA R package (v1.69) was used to construct an unsigned gene co-expression network with a soft threshold power [beta] of 6. Nineteen tightly connected modules were detected, while genes that were not connected to the 19 modules were collected in the 20th "grey" module. WGCNA defines the expression of a given module by averaging module gene expressions, which is also called module eigengene expression. Using a non-parametric Kruskal-Wallis test (p value < 0.05), we can identify modules that differ significantly among mouse samples with different genotypes. For example, the "Greenyellow" module differs significantly between zQ175 mice and zQ175:CK2α'$^{(+/-)}$ mice. Data for the Greenyellow module were exported using a Cytoscape format for visualization. Network figures are limited to the top 10% of genes with the strongest network connections (the topological overlap threshold was raised until only 10% of genes remained). The network modules are color coded by the differential expression between zQ175 mice and zQ175:CK2α'$^{(+/-)}$ mice: blue, downregulated in zQ175 compared to ZQ175:CK2α'$^{(+/-)}$ mice; red, upregulated in zQ175 compared to

747 ZQ175:CK2α'$^{(+/-)}$. The size of the circles is scaled by the absolute value of the mean
748 log2 fold change between zQ175 and ZQ175:CK2α'$^{(+/-)}$ mice.

749

750 **Quantification and Statistical analyses**

751 Data are expressed as Mean ± SEM, Mean ± SD, or percentage, analyzed for statistical
752 significance, and displayed by Prism 8 software (GraphPad, San Diego, CA) or Excel
753 software (Microsoft). Pearson correlation tests were applied to test the normal
754 distribution of experimental data. Normal distributions were compared with t-test (two-
755 tailed) or ANOVA with appropriate post-hoc tests (Sidak's, Dunn's, or Tukey's) for
756 multiple comparisons. Non-normal distributions were compared with the non-parametric
757 Kruskal-Wallis test with an appropriate post-hoc test, as indicated. The accepted level of
758 significance was $p \leq 0.05$, therefore samples indicated as n.s (no significant) did not
759 reach $p \leq 0.05$. Statistical analyses for electrophysiological experiments were performed
760 with SigmaPlot 13.0 software. No statistical methods were used to predetermine sample
761 sizes, but sample sizes were chosen to be similar to those reported in previous
762 publications [11]. In the figures, we show the mean as an estimator of central tendency
763 including when we have used a non-parametric test, to maintain consistency with other
764 figures in the paper and because it is more intuitive to compare the mean values.

765

766 **Acknowledgements**

767

768 We are grateful to Drs. Sylvain Lesne and Michael Lee for sharing his expertise on
769 alpha-synuclein and sharing reagents, Maha Syed and Joyce Meints for technical
770 assistance, Jason Mitchell for assistance with confocal microscopy and Erin Greguske
771 for proofreading.

772

773 **Authors' contributions**

774

775 R.G.P obtained funding for the study and designed the experiments. D.Y and N.Z,
776 harvested mice, conducted behavioral analyses, performed IF and conducted alpha-
777 synuclein related experiments. F.C conducted cytokine proteome profiling and astrocyte
778 IF analyses. J.Y performed EM48 and Neu analyses. T.B conducted microglia analyses.
779 W.T conducted IL6-related experiments and qRT-PCR of SNCA^{KO} mice. K.J performed
780 striatal qRT-PCR. H.K conducted striatal volume analyses. C.N conducted
781 electrophysiological experiments. T.S.M conducted behavioral analyses. K.G and S.L
782 performed MRS analyses. A.W conducted a-syn IB and nuclear/cytoplasma
783 fractionation. R.M assisted in IF image analyses and a-syn/EM48 puncta analyses.

C.T.Z prepared SNCA^{KO} tissues. Y.Z conducted RNA-seq analyses. D.Y, N.Z, R.M, S.L, K.G, C.N, W.T and R.G.P prepared and analyzed the data. G.O supervised the MR data acquisition and analysis. M.B supervised mouse behavioral data acquisition and analysis. A.A supervised electrophysiological recordings. M.C supervised microglia analyses. J.J.L supervised SNCA^{KO} tissue preparation. R.G.P wrote the first draft of the manuscript and all authors edited subsequent versions. All authors read and approved the final version of the manuscript.

Funding

This work was supported by R.G.P's startup funds from University of Minnesota, the Biomedical Research Awards for Interdisciplinary New Science BRAINS (to R.G.P) and the National Institute of Health NINDS (R01 NS110694-01A1) (to R.G.P). The Center for Magnetic Resonance Research is supported by the National Institute of Biomedical Imaging and Bioengineering (NIBIB) grant P41 EB027061, the Institutional Center Cores for Advanced Neuroimaging award P30 NS076408 and the W.M. Keck Foundation. F.C. received the mobility scholarship program Global Links: an Opportunity to Build a University Strategy 2018/2019 (GLOBUS Placement), Università degli Studi di Cagliari, funded through the Regione Autonoma della Sardegna. National Institute of Health NINDS (R01 NS197387) (to M.C.) and National Institute of Health NINDS R01 MH119355 and R01 NS108686 (to A.A). Grants from Fundación Ramón Areces, MICINN (SAF2009-08233) and MCIU/AEI/FEDER-UE (RTI2018-096322-B-100) to JJL.

Data availability

RNA-seq data sets have been deposited at GEO. Mouse models and reagents regenerated during the execution of this work are available upon request.

Declaration of interest

The authors declare no competing interests.

References

1. T. H. s. D. C. R. Group, A novel gene containing a trinucleotide repeat that is expanded and unstable on Huntington's disease chromosomes. *Cell* **72**, 971-983 (1993).
2. M. DiFiglia *et al.*, Aggregation of huntingtin in neuronal intranuclear inclusions and dystrophic neurites in brain. *Science* **277**, 1990-1993 (1997).

821 3. R. J. Ferrante, N. W. Kowall, E. P. Richardson, Proliferative and degenerative
822 changes in striatal spiny neurons in Huntington's disease: a combined study using the
823 section-Golgi method and calbindin D28k immunocytochemistry. *J Neurosci* **11**, 3877-
824 3887 (1991).
825 4. A. Crotti, C. K. Glass, The choreography of neuroinflammation in Huntington's
826 disease. *Trends Immunol* **36**, 364-373 (2015).
827 5. J. Castello, A. Ragnauth, E. Friedman, H. Rebholz, CK2-An Emerging Target for
828 Neurological and Psychiatric Disorders. *Pharmaceuticals (Basel)* **10** (2017).
829 6. A. F. Rosenberger *et al.*, Increased occurrence of protein kinase CK2 in
830 astrocytes in Alzheimer's disease pathology. *J.Neuroinflammation.* **13**, 4 (2016).
831 7. L. A. Pinna, Protein kinase CK2: a challenge to canons. *J.Cell Sci.* **115**, 3873-
832 3878 (2002).
833 8. D. W. Litchfield, Protein kinase CK2: structure, regulation and role in cellular
834 decisions of life and death. *Biochem.J.* **369**, 1-15 (2003).
835 9. Y. Bian *et al.*, Global screening of CK2 kinase substrates by an integrated
836 phosphoproteomics workflow. *Sci.Rep.* **3**, 3460 (2013).
837 10. I. Ceglia, M. Flajolet, H. Rebholz, Predominance of CK2α over CK2α' in the
838 mammalian brain. *Mol Cell Biochem* **356**, 169-175 (2011).
839 11. R. Gomez-Pastor *et al.*, Abnormal degradation of the neuronal stress-protective
840 transcription factor HSF1 in Huntington's disease. *Nat Commun* **8**, 14405 (2017).
841 12. R. Gomez-Pastor, E. T. Burchfiel, D. J. Thiele, Regulation of heat shock
842 transcription factors and their roles in physiology and disease. *Nat Rev Mol Cell Biol*
843 (2018).
844 13. M. M. Fan, H. Zhang, M. R. Hayden, S. L. Pelech, L. A. Raymond, Protective up-
845 regulation of CK2 by mutant huntingtin in cells co-expressing NMDA receptors. *J*
846 *Neurochem* **104**, 790-805 (2008).
847 14. R. S. Atwal *et al.*, Kinase inhibitors modulate huntingtin cell localization and
848 toxicity. *Nat.Chem.Biol.* **7**, 453-460 (2011).
849 15. J. A. Greenwood, C. W. Scott, R. C. Spreen, C. B. Caputo, G. V. Johnson,
850 Casein kinase II preferentially phosphorylates human tau isoforms containing an amino-
851 terminal insert. Identification of threonine 39 as the primary phosphate acceptor. *J Biol*
852 *Chem* **269**, 4373-4380 (1994).
853 16. E. Masliah *et al.*, Casein kinase II alteration precedes tau accumulation in tangle
854 formation. *Am.J.Pathol.* **140**, 263-268 (1992).
855 17. E. A. Waxman, B. I. Giasson, Specificity and regulation of casein kinase-
856 mediated phosphorylation of alpha-synuclein. *J Neuropathol Exp Neurol* **67**, 402-416
857 (2008).
858 18. C. Ising *et al.*, NLRP3 inflammasome activation drives tau pathology. *Nature* **575**,
859 669-673 (2019).
860 19. E. Masliah *et al.*, Dopaminergic loss and inclusion body formation in alpha-
861 synuclein mice: implications for neurodegenerative disorders. *Science* **287**, 1265-1269
862 (2000).
863 20. C. Tomás-Zapico *et al.*, α-Synuclein accumulates in huntingtin inclusions but
864 forms independent filaments and its deficiency attenuates early phenotype in a mouse
865 model of Huntington's disease. *Hum Mol Genet* **21**, 495-510 (2012).

21. M. Fernández-Nogales *et al.*, Huntington's disease is a four-repeat tauopathy with tau nuclear rods. *Nat Med* **20**, 881-885 (2014).
22. P. Liu *et al.*, A soluble truncated tau species related to cognitive dysfunction is elevated in the brain of cognitively impaired human individuals. *Sci Rep* **10**, 3869 (2020).
23. A. Shalash *et al.*, Elevated Serum α-Synuclein Autoantibodies in Patients with Parkinson's Disease Relative to Alzheimer's Disease and Controls. *Front Neurol* **8**, 720 (2017).
24. M. Breza *et al.*, Elevated Serum α-Synuclein Levels in Huntington's Disease Patients. *Neuroscience* **431**, 34-39 (2020).
25. S. Corrochano *et al.*, α-Synuclein levels affect autophagosome numbers in vivo and modulate Huntington disease pathology. *Autophagy* **8**, 431-432 (2012).
26. T. Heikkinen *et al.*, Characterization of neurophysiological and behavioral changes, MRI brain volumetry and 1H MRS in zQ175 knock-in mouse model of Huntington's disease. *PLoS One* **7**, e50717 (2012).
27. L. B. Menalled *et al.*, Comprehensive behavioral and molecular characterization of a new knock-in mouse model of Huntington's disease: zQ175. *PLoS One* **7**, e49838 (2012).
28. P. Arlotta, B. J. Molyneaux, D. Jabaudon, Y. Yoshida, J. D. Macklis, Ctip2 controls the differentiation of medium spiny neurons and the establishment of the cellular architecture of the striatum. *J Neurosci* **28**, 622-632 (2008).
29. N. N. Singh, D. P. Ramji, Protein kinase CK2, an important regulator of the inflammatory response? *J Mol Med (Berl)* **86**, 887-897 (2008).
30. F. B. Rodrigues *et al.*, Cerebrospinal Fluid Inflammatory Biomarkers Reflect Clinical Severity in Huntington's Disease. *PLoS One* **11**, e0163479 (2016).
31. N. Pavese *et al.*, Microglial activation correlates with severity in Huntington disease: a clinical and PET study. *Neurology* **66**, 1638-1643 (2006).
32. Y. F. Tai *et al.*, Imaging microglial activation in Huntington's disease. *Brain Res Bull* **72**, 148-151 (2007).
33. J. C. Savage *et al.*, Microglial physiological properties and interactions with synapses are altered at presymptomatic stages in a mouse model of Huntington's disease pathology. *J Neuroinflammation* **17**, 98 (2020).
34. K. Li, J. Li, J. Zheng, S. Qin, Reactive Astrocytes in Neurodegenerative Diseases. *Aging Dis* **10**, 664-675 (2019).
35. B. S. Khakh *et al.*, Unravelling and Exploiting Astrocyte Dysfunction in Huntington's Disease. *Trends Neurosci* **40**, 422-437 (2017).
36. M. Castillo, L. Kwock, J. Scatliff, S. K. Mukherji, Proton MR spectroscopy in neoplastic and non-neoplastic brain disorders. *Magn Reson Imaging Clin N Am* **6**, 1-20 (1998).
37. A. Brand, C. Richter-Landsberg, D. Leibfritz, Multinuclear NMR studies on the energy metabolism of glial and neuronal cells. *Dev Neurosci* **15**, 289-298 (1993).
38. I. Tkac *et al.*, Homeostatic adaptations in brain energy metabolism in mouse models of Huntington disease. *J Cereb Blood Flow Metab* **32**, 1977-1988 (2012).
39. Q. Peng *et al.*, Characterization of Behavioral, Neuropathological, Brain Metabolic and Key Molecular Changes in zQ175 Knock-In Mouse Model of Huntington's Disease. *PLoS One* **11**, e0148839 (2016).

912 40. S. A. Liddelow *et al.*, Neurotoxic reactive astrocytes are induced by activated
913 microglia. *Nature* **541**, 481-487 (2017).
914 41. L. E. Clarke *et al.*, Normal aging induces A1-like astrocyte reactivity. *Proc Natl*
915 *Acad Sci U S A* **115**, E1896-E1905 (2018).
916 42. S. K. Singhrao, J. W. Neal, B. P. Morgan, P. Gasque, Increased complement
917 biosynthesis by microglia and complement activation on neurons in Huntington's
918 disease. *Exp Neurol* **159**, 362-376 (1999).
919 43. B. Diaz-Castro, M. R. Gangwani, X. Yu, G. Coppola, B. S. Khakh, Astrocyte
920 molecular signatures in Huntington's disease. *Sci Transl Med* **11** (2019).
921 44. M. M. Zeron *et al.*, Increased sensitivity to N-methyl-D-aspartate receptor-
922 mediated excitotoxicity in a mouse model of Huntington's disease. *Neuron* **33**, 849-860
923 (2002).
924 45. A. I. Smith-Dijak, M. D. Sepers, L. A. Raymond, Alterations in synaptic function
925 and plasticity in Huntington disease. *J Neurochem* **150**, 346-365 (2019).
926 46. T. E. Wood *et al.*, Mutant huntingtin reduction in astrocytes slows disease
927 progression in the BACHD conditional Huntington's disease mouse model. *Hum Mol*
928 *Genet* **28**, 487-500 (2019).
929 47. T. Indersmitten, C. H. Tran, C. T. Cepeda, M. S. Levine, Altered Excitatory and
930 Inhibitory Inputs to Striatal Medium-Sized Spiny Neurons and Cortical Pyramidal
931 Neurons in the Q175 Mouse Model of Huntington's Disease. *J.Neurophysiol.*, jn (2015).
932 48. A. A. Fienberg *et al.*, DARPP-32: regulator of the efficacy of dopaminergic
933 neurotransmission. *Science* **281**, 838-842 (1998).
934 49. E. Vezzoli *et al.*, Inhibiting pathologically active ADAM10 rescues synaptic and
935 cognitive decline in Huntington's disease. *J Clin Invest* **129**, 2390-2403 (2019).
936 50. P. Langfelder *et al.*, Integrated genomics and proteomics define huntingtin CAG
937 length-dependent networks in mice. *Nat Neurosci* **19**, 623-633 (2016).
938 51. A. Gallardo-Orihuela *et al.*, Transcriptional correlates of the pathological
939 phenotype in a Huntington's disease mouse model. *Sci Rep* **9**, 18696 (2019).
940 52. G. M. o. H. s. D. G.-H. Consortium, Identification of Genetic Factors that Modify
941 Clinical Onset of Huntington's Disease. *Cell* **162**, 516-526 (2015).
942 53. M. Riessland *et al.*, Neurocalcin Delta Suppression Protects against Spinal
943 Muscular Atrophy in Humans and across Species by Restoring Impaired Endocytosis.
944 *Am J Hum Genet* **100**, 297-315 (2017).
945 54. O. Al-Dalahmah *et al.*, Single-nucleus RNA-seq identifies Huntington disease
946 astrocyte states. *Acta Neuropathol Commun* **8**, 19 (2020).
947 55. D. Davidi *et al.*, α-Synuclein Translocates to the Nucleus to Activate Retinoic-
948 Acid-Dependent Gene Transcription. *iScience* **23**, 100910 (2020).
949 56. M. Decressac *et al.*, α-Synuclein-induced down-regulation of Nurr1 disrupts
950 GDNF signaling in nigral dopamine neurons. *Sci Transl Med* **4**, 163ra156 (2012).
951 57. M. W. Rousseaux *et al.*, TRIM28 regulates the nuclear accumulation and toxicity
952 of both alpha-synuclein and tau. *Elife* **5** (2016).
953 58. A. Oueslati, Implication of Alpha-Synuclein Phosphorylation at S129 in
954 Synucleinopathies: What Have We Learned in the Last Decade? *J Parkinsons Dis* **6**,
955 39-51 (2016).
956 59. H. Fujiwara *et al.*, alpha-Synuclein is phosphorylated in synucleinopathy lesions.
957 *Nat.Cell Biol.* **4**, 160-164 (2002).

958 60. M. Mikula *et al.*, Halogenated imidazole derivatives block RNA polymerase II
959 elongation along mitogen inducible genes. *BMC Mol Biol* **11**, 4 (2010).
960 61. H. Y. Hsiao *et al.*, Inhibition of soluble tumor necrosis factor is therapeutic in
961 Huntington's disease. *Hum Mol Genet* **23**, 4328-4344 (2014).
962 62. S. Franciosi *et al.*, Age-dependent neurovascular abnormalities and altered
963 microglial morphology in the YAC128 mouse model of Huntington disease. *Neurobiol*
964 *Dis* **45**, 438-449 (2012).
965 63. K. W. Selmaj, M. Farooq, W. T. Norton, C. S. Raine, C. F. Brosnan, Proliferation
966 of astrocytes in vitro in response to cytokines. A primary role for tumor necrosis factor. *J*
967 *Immunol* **144**, 129-135 (1990).
968 64. H. Lian *et al.*, Astrocyte-Microglia Cross Talk through Complement Activation
969 Modulates Amyloid Pathology in Mouse Models of Alzheimer's Disease. *J Neurosci* **36**,
970 577-589 (2016).
971 65. K. Nilsson Ekdahl, B. Nilsson, Phosphorylation of complement component C3
972 after synthesis in U937 cells by a putative protein kinase, casein kinase 2, which is
973 regulated by CD11b: evidence that membrane-bound proteases preferentially cleave
974 phosphorylated C3. *Biochem J* **328 (Pt 2)**, 625-633 (1997).
975 66. A. Mottahedin *et al.*, Effect of Neuroinflammation on Synaptic Organization and
976 Function in the Developing Brain: Implications for Neurodevelopmental and
977 Neurodegenerative Disorders. *Front Cell Neurosci* **11**, 190 (2017).
978 67. C. Franchin *et al.*, Re-evaluation of protein kinase CK2 pleiotropy: new insights
979 provided by a phosphoproteomics analysis of CK2 knockout cells. *Cell Mol Life Sci* **75**,
980 2011-2026 (2018).
981 68. S. Hara *et al.*, Serine 129 phosphorylation of membrane-associated α-synuclein
982 modulates dopamine transporter function in a G protein-coupled receptor kinase-
983 dependent manner. *Mol Biol Cell* **24**, 1649-1660, S1641-1643 (2013).
984 69. G. Lee *et al.*, Casein kinase II-mediated phosphorylation regulates alpha-
985 synuclein/synphilin-1 interaction and inclusion body formation. *J Biol Chem* **279**, 6834-
986 6839 (2004).
987 70. C. Y. Chung, J. B. Koprich, H. Siddiqi, O. Isacson, Dynamic changes in
988 presynaptic and axonal transport proteins combined with striatal neuroinflammation
989 precede dopaminergic neuronal loss in a rat model of AAV alpha-synucleinopathy. *J*
990 *Neurosci* **29**, 3365-3373 (2009).
991 71. X. Xu, P. A. Toselli, L. D. Russell, D. C. Seldin, Globozoospermia in mice lacking
992 the casein kinase II alpha' catalytic subunit. *Nat.Genet.* **23**, 118-121 (1999).
993 72. A. Cavaccini, C. Durkee, P. Kofuji, R. Tonini, A. Araque, Astrocyte Signaling
994 Gates Long-Term Depression at Corticostriatal Synapses of the Direct Pathway. *J*
995 *Neurosci* **40**, 5757-5768 (2020).
996 73. G. Öz *et al.*, Assessing recovery from neurodegeneration in spinocerebellar
997 ataxia 1: Comparison of in vivo magnetic resonance spectroscopy with motor testing,
998 gene expression and histology. *Neurobiol Dis* **74**, 158-166 (2015).
999 74. A. M. Bolger, M. Lohse, B. Usadel, Trimmomatic: a flexible trimmer for Illumina
1000 sequence data. *Bioinformatics* **30**, 2114-2120 (2014).
1001 75. P. Langfelder, S. Horvath, WGCNA: an R package for weighted correlation
1002 network analysis. *BMC Bioinformatics* **9**, 559 (2008).

1003

1004 **Figure Legends**

1005

1006 **Figure 1**. **CK2α' levels progressively increase in the striatum of zQ175 and**
1007 **correlate with HTT aggregation and NeuN depletion.** ***A***, ***B,*** Immunostaining and
1008 quantification of HTT puncta detected with anti-HTT EM48 antibody, ***C***, ***D***, NeuN$^+$ cells
1009 and ***E***, ***F***, CK2α' levels in zQ175 compared with WT mice at 3, 6, 12 and 22 months
1010 (*n*=6 mice/genotype). ***G,*** CK2α' mRNA levels analyzed by RT-qPCR in striatum and
1011 cortex of 6 month old mice. Data was normalized to GAPDH and WT striatum (n=3
1012 mice/genotype). ***H***, Linear regression analysis between CK2α' levels and HTT puncta,
1013 and ***I***, between CK2α' levels and number of NeuN$^+$ cells in zQ175 mice. The Pearson
1014 correlation coefficient (ρ) and R^2 are indicated. Data are mean ± SD with significance
1015 determined by one-way ANOVA Dunnett's post-hoc test in ***B*** and ***F*** and two-way
1016 ANOVA Tukey post-hoc test in ***D*** and ***G***. p-values <0.05 are indicated. n.s = not
1017 significant. Scale bar, 50 μm.

1018

1019 **Figure 2**. **Expression of pro-inflammatory cytokines in the striatum of zQ175 is**
1020 **decreased by reduction in CK2α'**. ***A***, RT-qPCR analysis for CK2α' and IL-6 in
1021 immortalized embryonic striatal cells ST*Hdh*$^{Q7/Q7}$ (control) and ST*Hdh*$^{Q111/Q111}$ (HD) (n =
1022 5 independent experiments). Data were normalized to GAPDH and using control cells
1023 as a reference. ***B***, siRNA knockdown of CK2α' for 24 h in ST*Hdh*$^{Q111/Q111}$ cells and RT-
1024 qPCR. Data were normalized with GAPDH and relativized to non-targeting control
1025 siRNA-treated cells (scramble), (*n* = 6 independent experiments). Data are mean ± SEM
1026 with significance determined by paired Student's t-test. ***C***, ***D***, Representative IF images
1027 and quantitative analysis of CK2α' in striatal MSNs immunostained for Ctip2, a specific
1028 MSN marker, in WT, zQ175 and zQ175:CK2α' $^{(+/-)}$ mice at 12 months of age (*n*=6
1029 mice/genotype). Scale bar, 50 μm. ***E***, ***F***, Representative images of mouse cytokine
1030 array panels in striatum extracts of WT, zQ175, and zQ175:CK2α'$^{(+/-)}$ at 12-14 months of
1031 age (*n* = 6 mice/genotype). ***G-I***, Iba1 IB in the striatum of 12 months old WT, zQ175 and
1032 zQ175:CK2α'. Quantification was measured by image analyses using Image J
1033 software. Scale bar, 100 μm. Error bars denote mean ± SD, values were analyzed by
1034 Student's t test in ***F***, and one-way ANOVA and Tukey post-hoc test in ***A, B, D***, and ***H***. **p*
1035 represent p-values comparing zQ175 and WT, #*p* are p-values comparing zQ175 and
1036 zQ175:CK2α'$^{(+/-)}$.

1037

1038 **Figure 3**. **Decreased CK2α' ameliorated astrocyte pathology in zQ175 mice**. ***A***,
1039 Representative images of striatum sections from 12-month-old mice immunostained for
1040 CK2α' and glutamine synthetase (GS, an astrocytic marker) in WT, zQ175 and
1041 zQ175:CK2α'$^{(+/-)}$. ***B***, Quantification of GS$^+$ cells from images in ***A*** (*n* = 5 mice/genotype).
1042 ***C***, Representative coronal images of brain scans in 9.4T magnet showing the striatum
1043 voxel (green box) for MRS acquisition from each genotype at 22 months of age. ***D***, *myo*-
1044 inositol (Ins) quantification in WT, zQ175 and zQ175:CK2α'$^{(+/-)}$ (*n* = 4-6
1045 mice/genotype). ***E***, Representative IF analysis of C3d co-stained with GS in the
1046 striatum of 12-month-old mice. ***E'***, Higher magnification of the outlined section in ***E***

1047 shows a representative view of a single astrocyte immunolabeled with C3d and GS. ***F,***
1048 Quantification of C3d signal from images in ***E***. ***G***, Quantification of $C3d^+$ GS^+ double-
1049 positive cells (*n* = 5 mice/genotype). DAPI is used for nuclear staining. Scale bars, 50
1050 µm. Error bars denote mean ± SD. *p*-values for differences between groups are
1051 indicated in each graph and calculated using two-way ANOVA and Tukey post-hoc
1052 tests. n.s. = not significant.

1053

1054 **Figure 4**. **CK2α' haploinsufficiency increased the frequency of AMPA-mediated**
1055 **miniature excitatory postsynaptic currents (mEPSC) in the dorsolateral striatum**
1056 **of zQ175 mice**. ***A***, Image shows whole-cell patch-clamp recording diagram in acute
1057 dorsolateral striatum slices, where Ctip2 labeled MSNs from 12-month-old mice. Scale
1058 bar 500 µm, Ctr: Cortex; Str: Striatum. ***B***, Input–output curve (WT, n = 8; zQ175, n = 9;
1059 zQ175:CK2α'$^{(+/-)}$ n = 13). Representative traces are shown in the top inset. ***C***, Short-
1060 term potentiation measured via paired-pulse facilitation (WT, n = 8; zQ175, n = 9;
1061 zQ175:CK2α'$^{(+/-)}$ n = 11). Representative traces of two consecutive stimuli delivered at
1062 25 ms time intervals are shown in the top inset. ***D***, Short-term depression analyzed
1063 through synaptic fatigue (WT, n = 7; zQ175, n = 9; zQ175:CK2α'$^{(+/-)}$ n = 12).
1064 Representative traces are shown in the top inset. Values were analyzed using two-way
1065 ANOVA with Tukey's post-hoc analysis. ***E-F***, Spontaneous recordings of mini excitatory
1066 postsynaptic currents (mEPSCs). Amplitude (in pA; left panel) and frequency (in Hz;
1067 right panel) were analyzed (WT, n = 10; zQ175, n = 9; zQ175:CK2α'$^{(+/-)}$ n = 12). ***G***,
1068 Representative mEPSC traces. Values were analyzed using one-way ANOVA with
1069 Dunn´s post-hoc analysis. P values <0.05 are indicated. Error bars represent mean ±
1070 SEM from at least 3 mice/genotype.

1071

1072 **Figure 5**. **Genetic deletion of CK2α' improved motor deficits in zQ175.** ***A***, Number
1073 of foot slips recorded while walking on four different types of beams with different
1074 degrees of difficulty from less to more challenging; medium-square, medium round,
1075 small-square and small-round (Beam test), and ***B***, Latency to fall off the rod Rotarod
1076 test) at 3, 6 and 12 months of age (n =16-18 mice/genotype in 3 months, n= 12-14 for 6
1077 months and n = 5-6 for 12 months). Error bars denote mean ± SEM, values were
1078 analyzed by two-way ANOVA with *Sidak's* post-hoc test. p-values <0.05 are indicated,
1079 n.s = not significant.

1080

1081 **Figure 6**. **Depletion of CK2α' restored the expression of synaptic genes**
1082 **associated with α-syn-dependent regulation in the striatum of symptomatic zQ175**
1083 **mice**. ***A***, Kruskal-Wallis test of module expressions between zQ175 (HD) mice and
1084 zQ175:CK2α'$^{(+/-)}$ mice. The y-axis is the negative log transformed p-values. ***B***,
1085 Expressions of module "Greenyellow" in each mouse sample. ***C***, IPA canonical pathway
1086 analysis of module genes for module "Greenyellow". ***D***, Enrichment analysis of GO
1087 terms in CC (cellular component) for module genes of module "Greenyellow". ***E***,
1088 Network visualization of top 15% connected genes in "Greenyellow" Module. The size of
1089 the circles was scaled by the absolute value of the mean log2-fold change between

1090 zQ175 and zQ175:CK2α'$^{(+/-)}$ mice. ***F***, Marker genes and their mean log2 fold change
1091 between zQ175 and zQ175:CK2α'$^{(+/-)}$ mice compared to WT. ***G***, IPA network analysis of
1092 DGEs in zQ175:CK2α' mice showing α-syn as the most significant upstream regulator.

1093

1094 **Figure 7. α-syn differentially accumulates in the nucleus of symptomatic zQ175**
1095 **mice and colocalized with mtHTT**. ***A,*** α-syn (4D6 antibody) IB in the striatum of WT,
1096 zQ175 and SNCA^{KO} and ***B*** in WT, zQ175 and zQ175:CK2α'$^{(+/-)}$ mice at 12 months old.
1097 GAPDH used as loading control. ***C,*** α-syn protein levels analyzed by Image J from IB
1098 analyses (n= 5-6 mice/genotype). ***D,*** Nuclear/cytoplasmic fractionation of striatum
1099 samples from 12-month-old WT, zQ175 and SNCA^{KO} mice. ***E***, Quantification of nuclear
1100 α-syn from images in D (n=4 mice/genotype). ***F***, Representative IF images of dorsal
1101 striatum sections from 12 month old WT, zQ175 and zQ175:CK2α'$^{(+/-)}$ (n=3
1102 mice/genotype) for α-syn and HTT (EM48 antibody). White arrows indicate α-syn/HTT
1103 colocalization. Scale bar, 10 μm. ***G,*** Magnification of images from F showing nuclear
1104 and cytoplasmic α-syn and HTT colocalization. Grey circles represent nuclei. White
1105 arrows indicate α-syn/HTT colocalization. Scale bar, 2 μm. ***H*** Number of cytoplasmic
1106 and ***I*** nuclear EM48^{+} puncta calculated using Image J Puncta analysis plugin. A total of
1107 three images per brain section and three brain sections per genotype were analyzed
1108 (n=27 images, n=3 mice/ genotype). ***J***, Number of colocalized α-syn and EM48^{+} puncta
1109 calculated using Image J Puncta analysis plugin (n=3 mice/genotype). Error bars denote
1110 mean ± SEM, values were analyzed by Student's t-test.

1111

1112 **Figure 8. CK2α' regulates phosphorylation of S129-α-syn and nuclear**
1113 **accumulation in symptomatic zQ175 mice**. ***A,*** pS129-α-syn (EP1536Y antibody) IB in
1114 the striatum of 12-month-old WT, zQ175 and SNCA^{KO} (n=4 mice/genotype)***.*** ***B*** pS129-α-
1115 syn (81A antibody) IB in the striatum of patients with HD (Vonsattel grade 3 and 4)
1116 compared to age and sex matched controls. GAPDH is used as loading control. ***C***
1117 pS129-α-syn protein levels analyzed by Image J from images in ***B***. Samples from grade
1118 3 and grade 4 HD were all grouped for pS129-α-syn quantification. ***D***, Representative
1119 pS129-α-syn IF images (81A antibody) in the dorsal striatum of 12-month-old WT,
1120 zQ175 and zQ175:CK2α'$^{(+/-)}$ (n=3 mice/genotype), Scale bar, 20 μm. ***E,*** pS129-α-syn
1121 fluorescence signal was calculated using Image J from images in D (n=3
1122 mice/genotype, n=27 images per mouse). ***F***, Magnification of images in D showed
1123 pS129-α-syn and EM48 colocalization in zQ175 and zQ175:CK2α'$^{(+/-)}$ (n=3 mice/group).
1124 ***G***, Quantification of pS129-α-syn and EM48 colocalized puncta using Image J puncta
1125 plug in. All data are mean ± SEM. Statistical analyses were conducted by one-way
1126 ANOVA. ***H***, Working model for the role of CK2α' in the regulation of pS129-α-syn and
1127 HD-like phenotype.

1128

1129

1130

1131

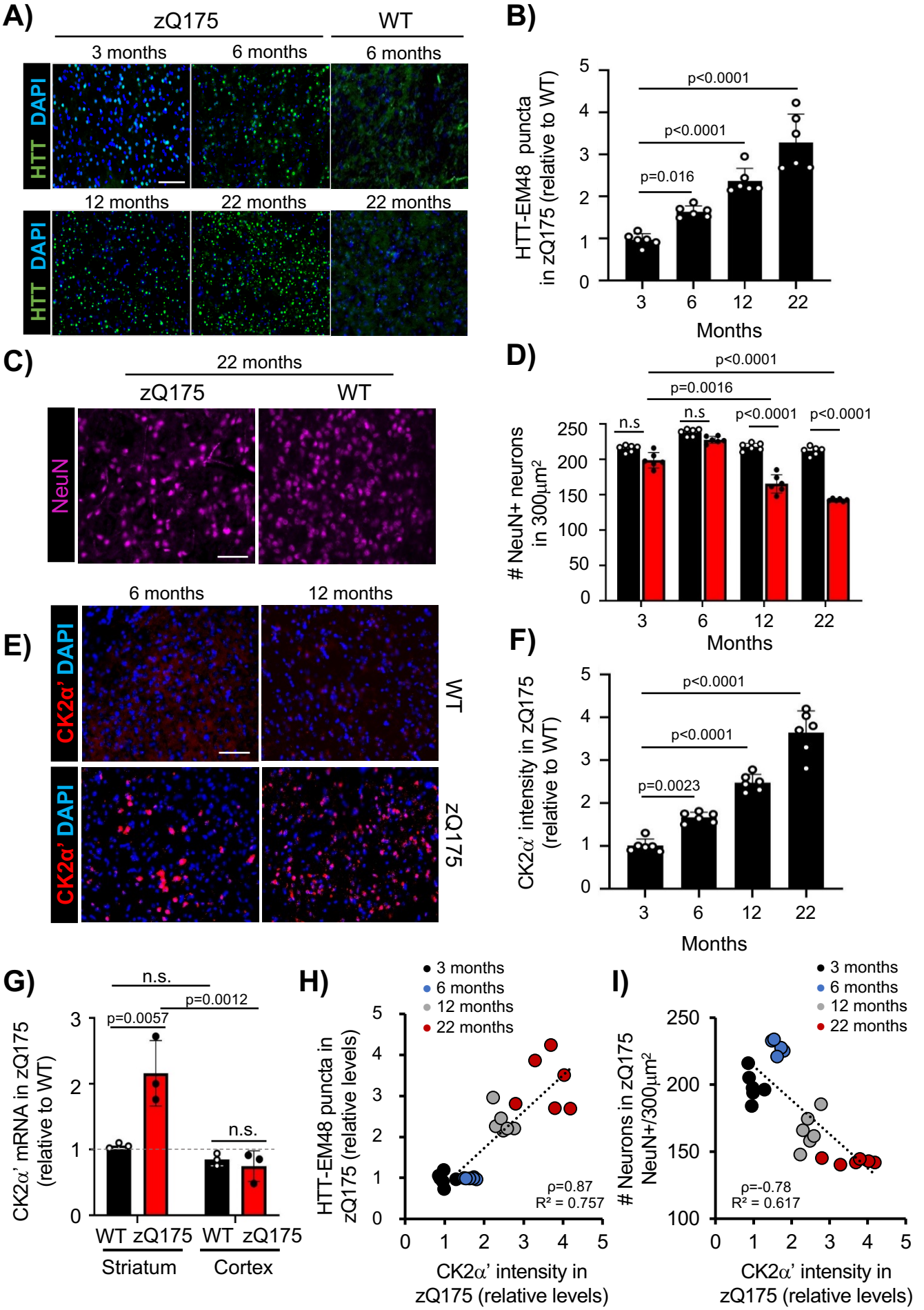
A)
zQ175
WT
3 months
6 months
6 months
HTT DAPI
12 months
22 months
22 months
HTT DAPI
B)
HTT-EM48 puncta in zQ175 (relative to WT)
p<0.0001
p<0.0001
p=0.016
Months
C)
22 months
zQ175
WT
NeuN
D)
NeuN+ neurons in 300µm²
p<0.0001
p=0.0016
n.s
n.s
p<0.0001
p<0.0001
Months
E)
6 months
12 months
CK2α' DAPI
WT
zQ175
F)
CK2α' intensity in zQ175 (relative to WT)
p<0.0001
p<0.0001
p=0.0023
Months
G)
CK2α' mRNA in zQ175 (relative to WT)
n.s.
p=0.0012
p=0.0057
n.s.
WT zQ175 WT zQ175
Striatum
Cortex
H)
3 months
6 months
12 months
22 months
HTT-EM48 puncta in zQ175 (relative levels)
ρ=0.87
R² = 0.757
CK2α' intensity in zQ175 (relative levels)
I)
3 months
6 months
12 months
22 months
Neurons in zQ175 NeuN+/300µm²
ρ=-0.78
R² = 0.617
CK2α' intensity in zQ175 (relative levels)

Figure 1

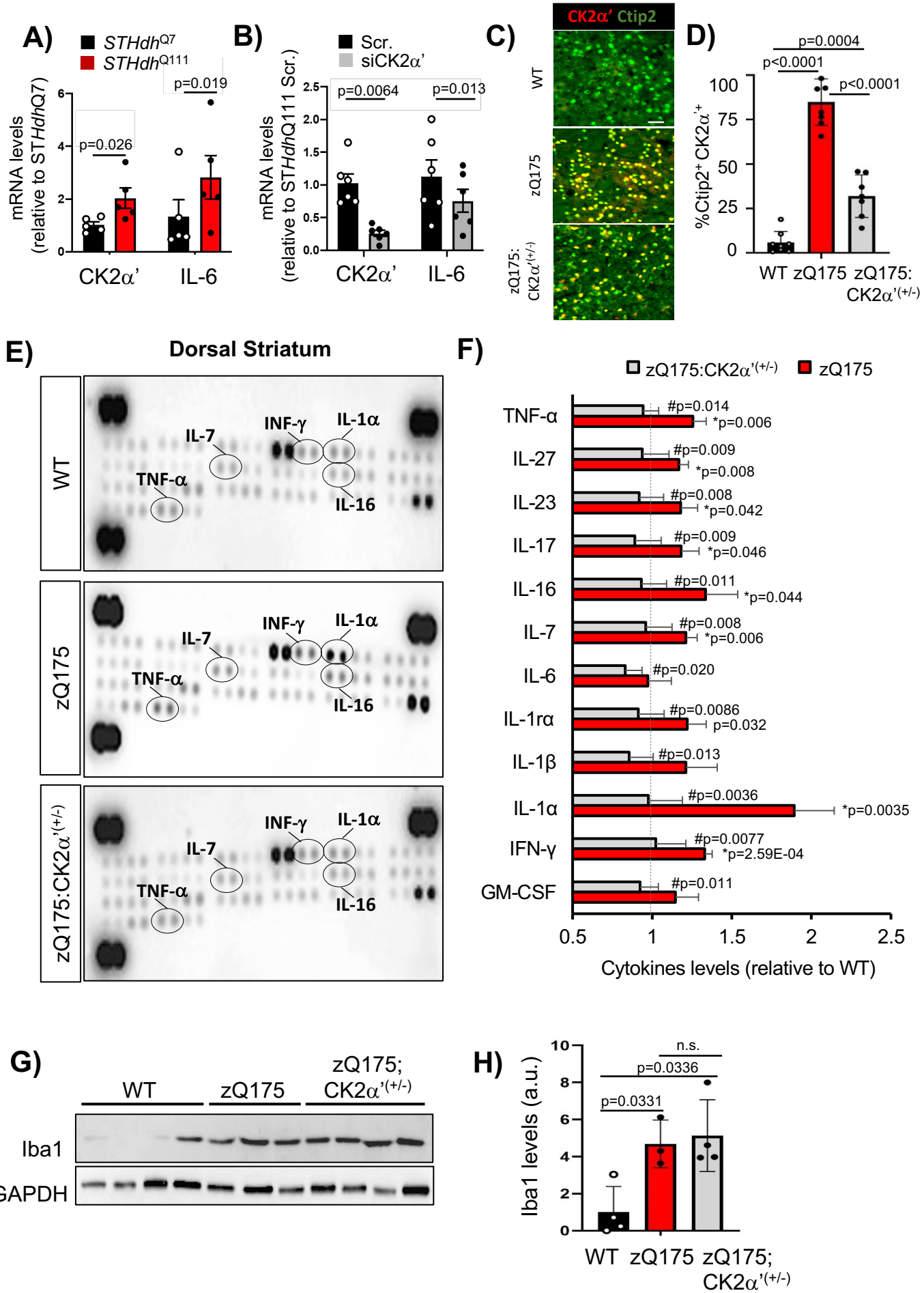
A)
STHdhQ7
STHdhQ111
mRNA levels (relative to STHdhQ7)
p=0.026
p=0.019
CK2α'
IL-6
B)
Scr.
siCK2α'
mRNA levels (relative to STHdhQ111 Scr.)
p=0.0064
p=0.013
CK2α'
IL-6
C)
CK2α' Ctip2
WT
zQ175
zQ175: CK2α'(+/-)
D)
p=0.0004
p<0.0001
p<0.0001
%Ctip2+ CK2α'+
WT zQ175 zQ175: CK2α'(+/-)
E)
Dorsal Striatum
WT
zQ175
zQ175:CK2α'(+/-)
IL-7
INF-γ
IL-1α
TNF-α
IL-16
F)
zQ175:CK2α'(+/-)
zQ175
TNF-α #p=0.014 *p=0.006
IL-27 #p=0.009 *p=0.008
IL-23 #p=0.008 *p=0.042
IL-17 #p=0.009 *p=0.046
IL-16 #p=0.011 *p=0.044
IL-7 #p=0.008 *p=0.006
IL-6 #p=0.020
IL-1rα #p=0.0086 p=0.032
IL-1β #p=0.013
IL-1α #p=0.0036 *p=0.0035
IFN-γ #p=0.0077 *p=2.59E-04
GM-CSF #p=0.011
Cytokines levels (relative to WT)
G)
WT
zQ175
zQ175; CK2α'(+/-)
Iba1
GAPDH
H)
n.s.
p=0.0336
p=0.0331
Iba1 levels (a.u.)
WT zQ175 zQ175; CK2α'(+/-)

Figure 2

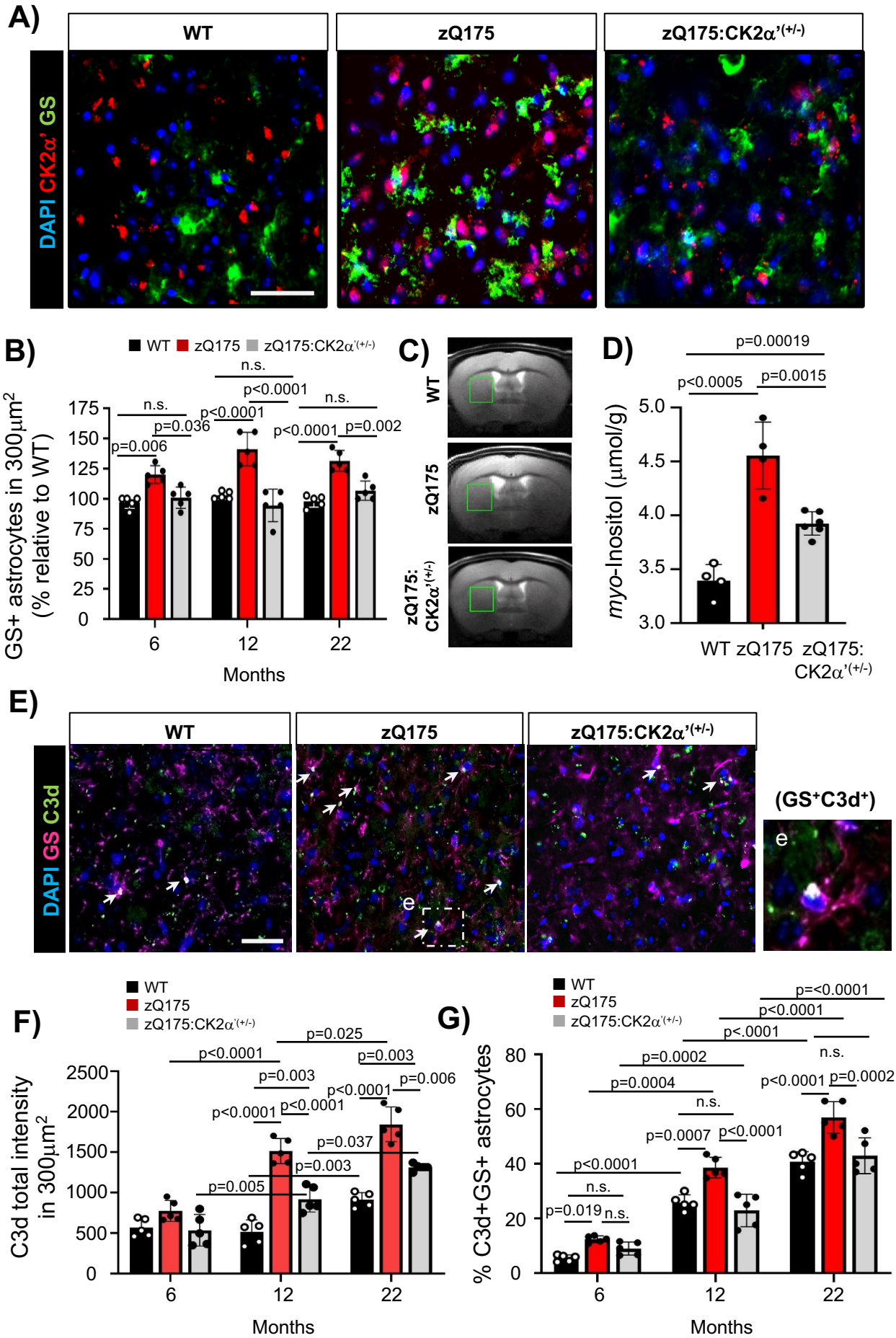
A)
WT
zQ175
zQ175:CK2α'(+/-)
DAPI CK2α' GS
B)
WT zQ175 zQ175:CK2α'(+/-)
GS+ astrocytes in 300μm2 (% relative to WT)
n.s.
p<0.0001
n.s.
p=0.036
p<0.0001
p=0.006
p<0.0001
p=0.002
Months
C)
WT
zQ175
zQ175: CK2α'(+/-)
D)
p=0.00019
p<0.0005
p=0.0015
myo-Inositol (μmol/g)
WT zQ175 zQ175: CK2α'(+/-)
E)
WT
zQ175
zQ175:CK2α'(+/-)
DAPI GS C3d
(GS+C3d+)
F)
WT
zQ175
zQ175:CK2α'(+/-)
C3d total intensity in 300μm2
p=0.025
p<0.0001
p=0.003
p=0.003
p=0.006
p<0.0001
p<0.0001
p<0.0001
p=0.037
p=0.003
p=0.005
Months
G)
WT
zQ175
zQ175:CK2α'(+/-)
% C3d+GS+ astrocytes
p=<0.0001
p<0.0001
p<.0001
n.s.
p=0.0002
p=0.0004
n.s.
p<0.0001
p=0.0002
p=0.0007
p<0.0001
p<0.0001
n.s.
p=0.019
n.s.
Months

Figure 3

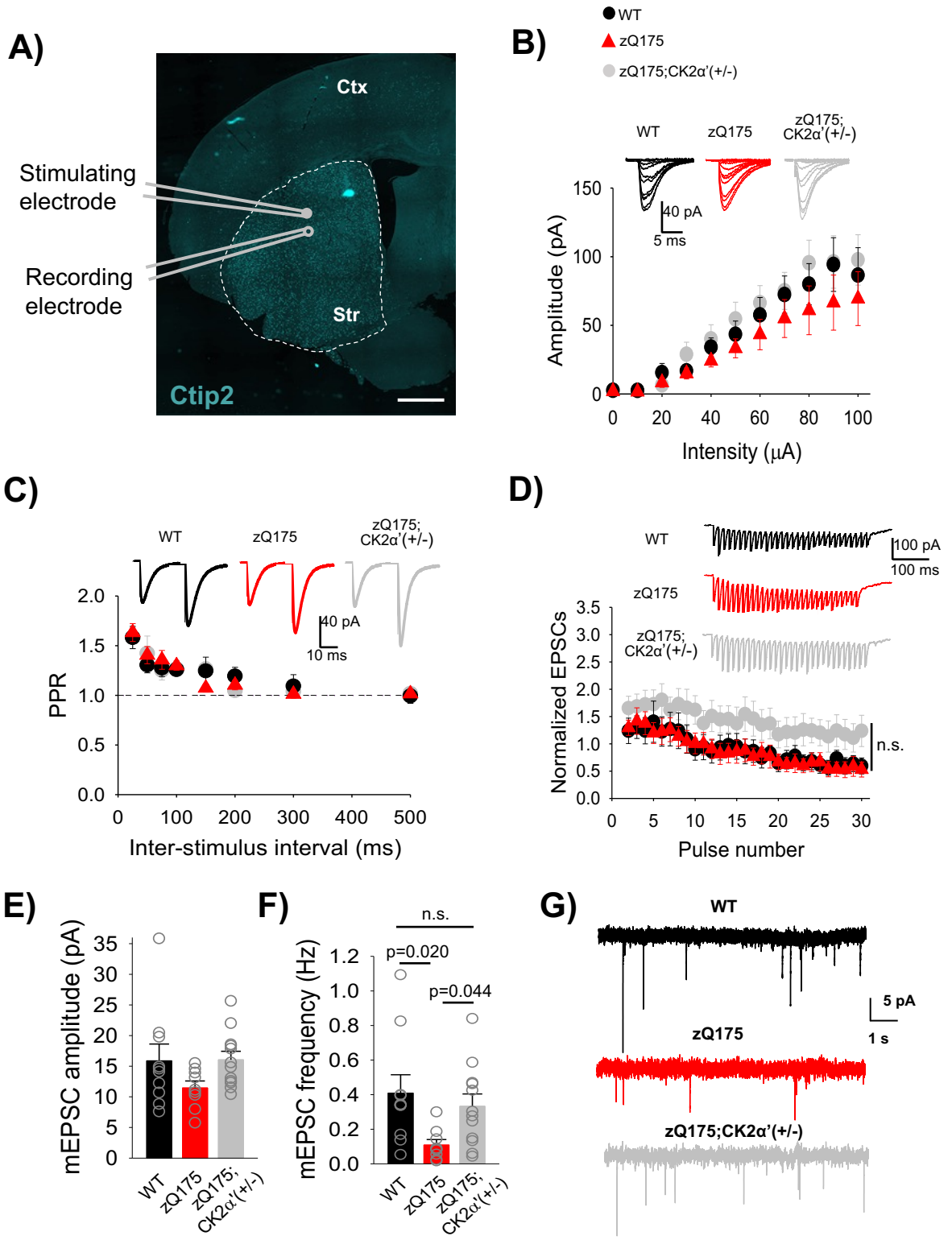
A)
Ctx
Stimulating electrode
Recording electrode
Str
Ctip2
B)
WT
zQ175
zQ175;CK2α'(+/-)
WT
zQ175
zQ175; CK2α'(+/-)
40 pA
5 ms
Amplitude (pA)
Intensity (μA)
C)
WT
zQ175
zQ175; CK2α'(+/-)
40 pA
10 ms
PPR
Inter-stimulus interval (ms)
D)
WT
zQ175
zQ175; CK2α'(+/-)
100 pA
100 ms
n.s.
Normalized EPSCs
Pulse number
E)
mEPSC amplitude (pA)
WT
zQ175
zQ175; CK2α'(+/-)
F)
n.s.
p=0.020
p=0.044
mEPSC frequency (Hz)
WT
zQ175
zQ175; CK2α'(+/-)
G)
WT
zQ175
zQ175;CK2α'(+/-)
5 pA
1 s

Figure 4

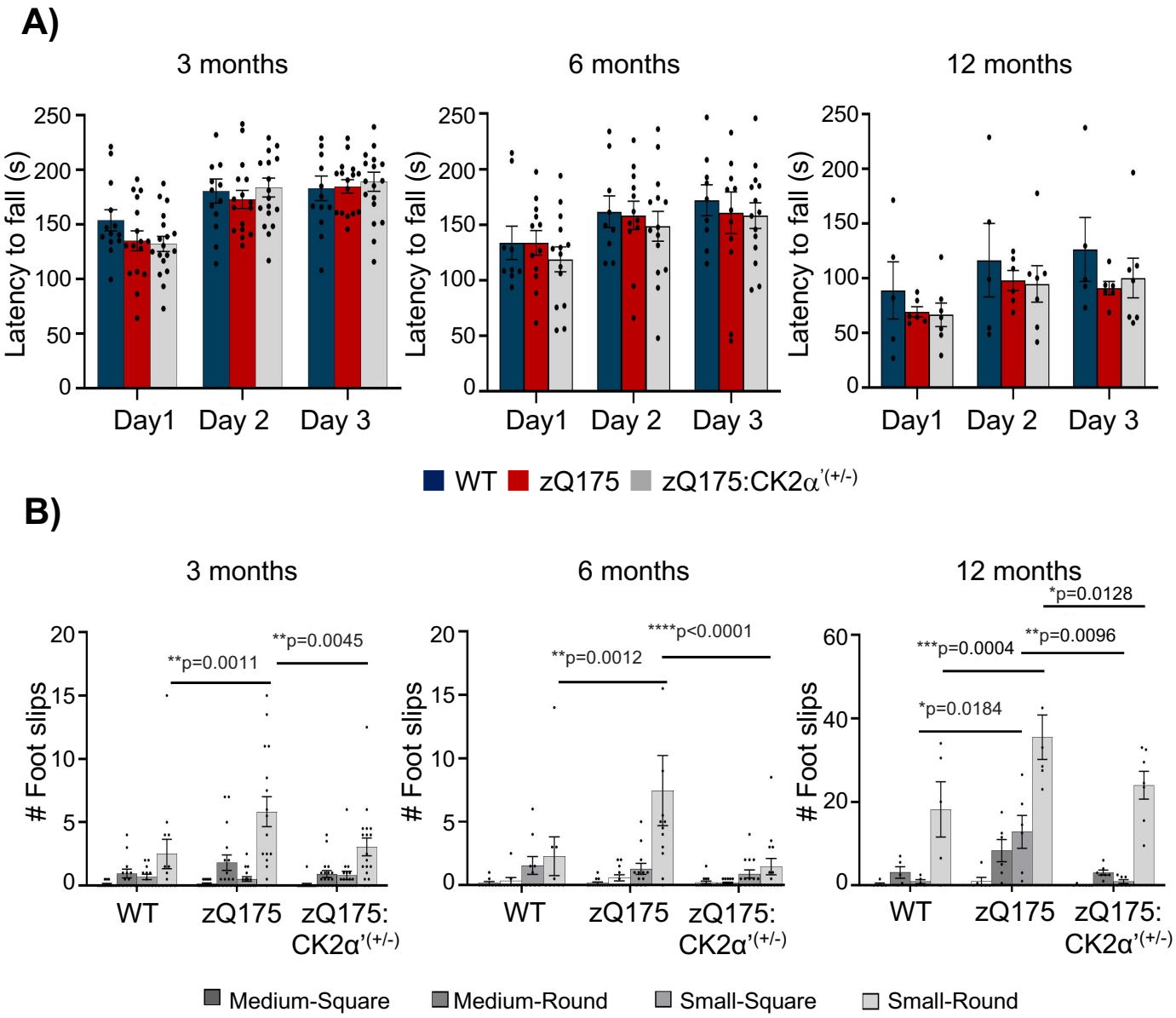
A)
3 months
6 months
12 months
Latency to fall (s)
250
200
150
100
50
0
Day1
Day 2
Day 3
WT
zQ175
zQ175:CK2α'(+/-)
B)
Foot slips
20
15
10
5
0
60
40
**p=0.0011
**p=0.0045
**p=0.0012
****p<0.0001
***p=0.0004
**p=0.0096
*p=0.0128
*p=0.0184
WT
zQ175
zQ175:
CK2α'(+/-)
Medium-Square
Medium-Round
Small-Square
Small-Round

Figure 5

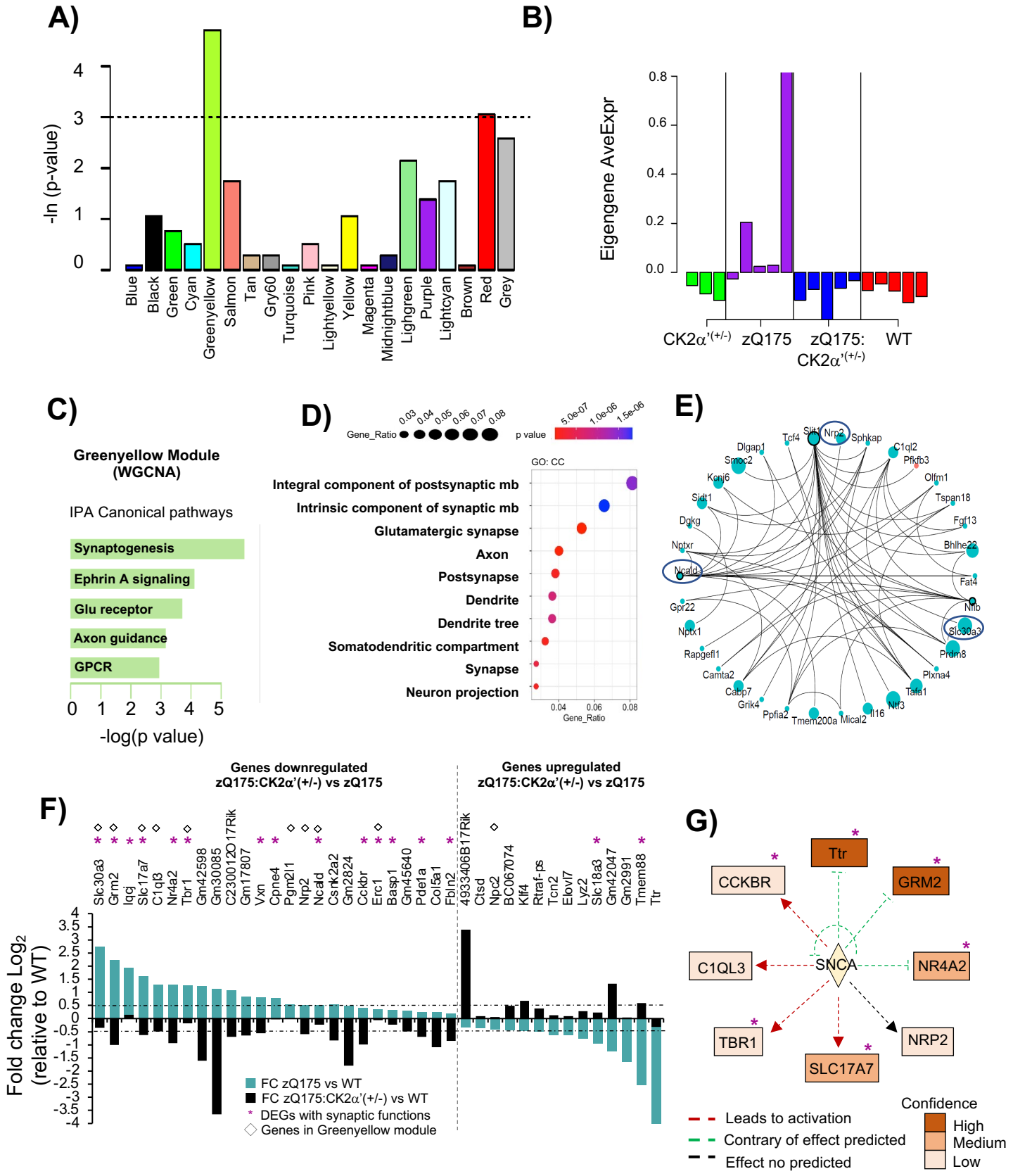
A)
-ln (p-value)
Blue
Black
Green
Cyan
Greenyellow
Salmon
Tan
Gry60
Turquoise
Pink
Lightyellow
Yellow
Magenta
Midnightblue
Lighgreen
Purple
Lightcyan
Brown
Red
Grey
B)
Eigengene AveExpr
CK2α'(+/-)
zQ175
zQ175: CK2α'(+/-)
WT
C)
Greenyellow Module (WGCNA)
IPA Canonical pathways
Synaptogenesis
Ephrin A signaling
Glu receptor
Axon guidance
GPCR
-log(p value)
D)
Gene_Ratio
p value
GO: CC
Integral component of postsynaptic mb
Intrinsic component of synaptic mb
Glutamatergic synapse
Axon
Postsynapse
Dendrite
Dendrite tree
Somatodendritic compartment
Synapse
Neuron projection
E)
F)
Genes downregulated zQ175:CK2α'(+/-) vs zQ175
Genes upregulated zQ175:CK2α'(+/-) vs zQ175
Fold change Log2 (relative to WT)
FC zQ175 vs WT
FC zQ175:CK2α'(+/-) vs WT
DEGs with synaptic functions
Genes in Greenyellow module
G)
Ttr
CCKBR
GRM2
C1QL3
SNCA
NR4A2
TBR1
SLC17A7
NRP2
Leads to activation
Contrary of effect predicted
Effect no predicted
Confidence
High
Medium
Low

Figure 6

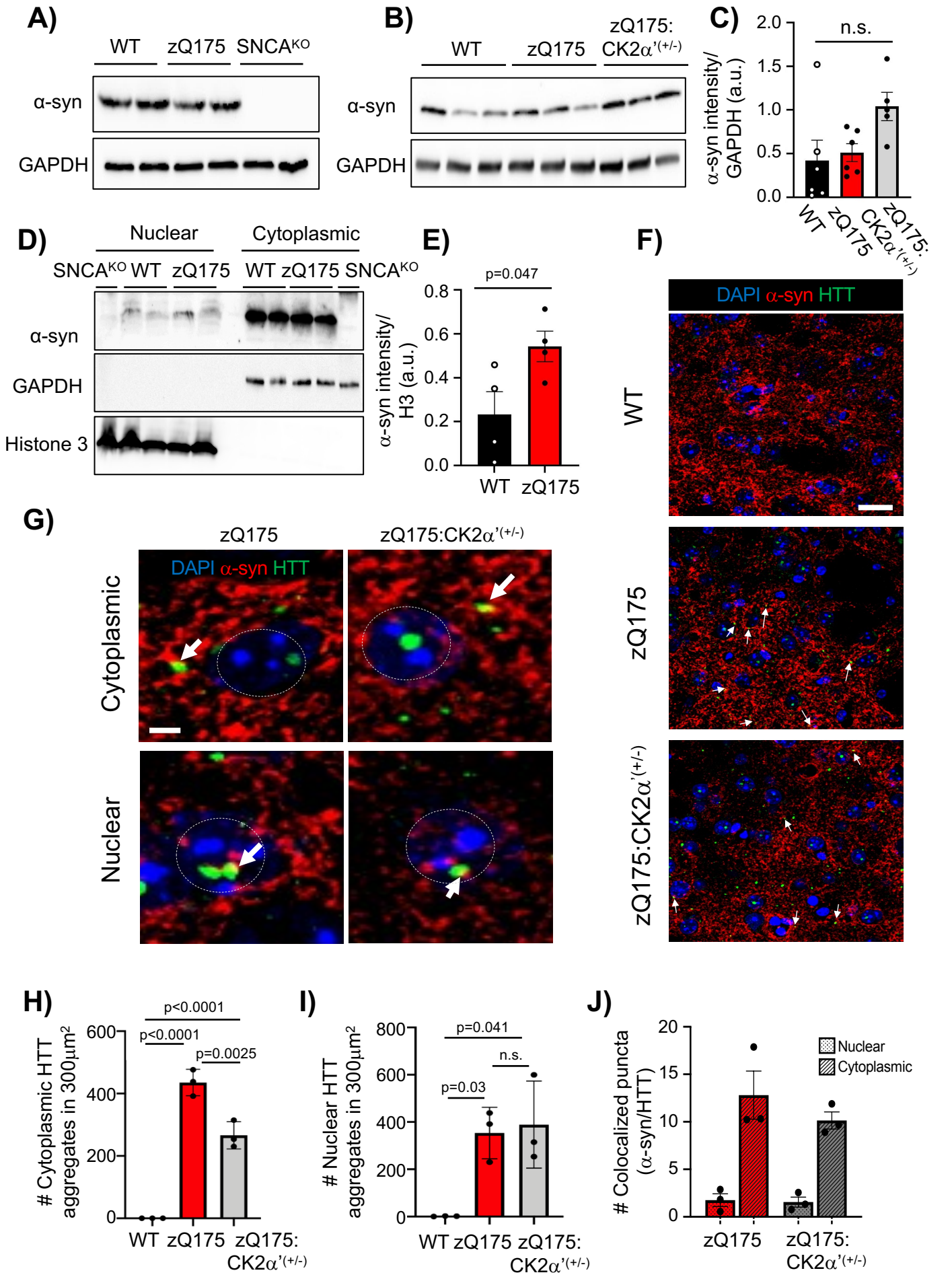
A)
WT
zQ175
SNCA^KO
α-syn
GAPDH
B)
WT
zQ175
zQ175: CK2α'(+/-)
α-syn
GAPDH
C)
n.s.
α-syn intensity/ GAPDH (a.u.)
2.0
1.5
1.0
0.5
0.0
WT
zQ175
zQ175: CK2α'(+/-)
D)
Nuclear
Cytoplasmic
SNCA^KO WT zQ175 WT zQ175 SNCA^KO
α-syn
GAPDH
Histone 3
E)
p=0.047
α-syn intensity/ H3 (a.u.)
0.8
0.6
0.4
0.2
0.0
WT
zQ175
F)
DAPI α-syn HTT
WT
zQ175
zQ175:CK2α'(+/-)
G)
zQ175
zQ175:CK2α'(+/-)
DAPI α-syn HTT
Cytoplasmic
Nuclear
H)
p<0.0001
p<0.0001
p=0.0025
# Cytoplasmic HTT aggregates in 300μm²
600
400
200
0
WT
zQ175
zQ175: CK2α'(+/-)
I)
p=0.041
n.s.
p=0.03
# Nuclear HTT aggregates in 300μm²
800
600
400
200
0
WT
zQ175
zQ175: CK2α'(+/-)
J)
Nuclear
Cytoplasmic
Colocalized puncta (α-syn/HTT)
20
15
10
5
0
zQ175
zQ175: CK2α'(+/-)

Figure 7

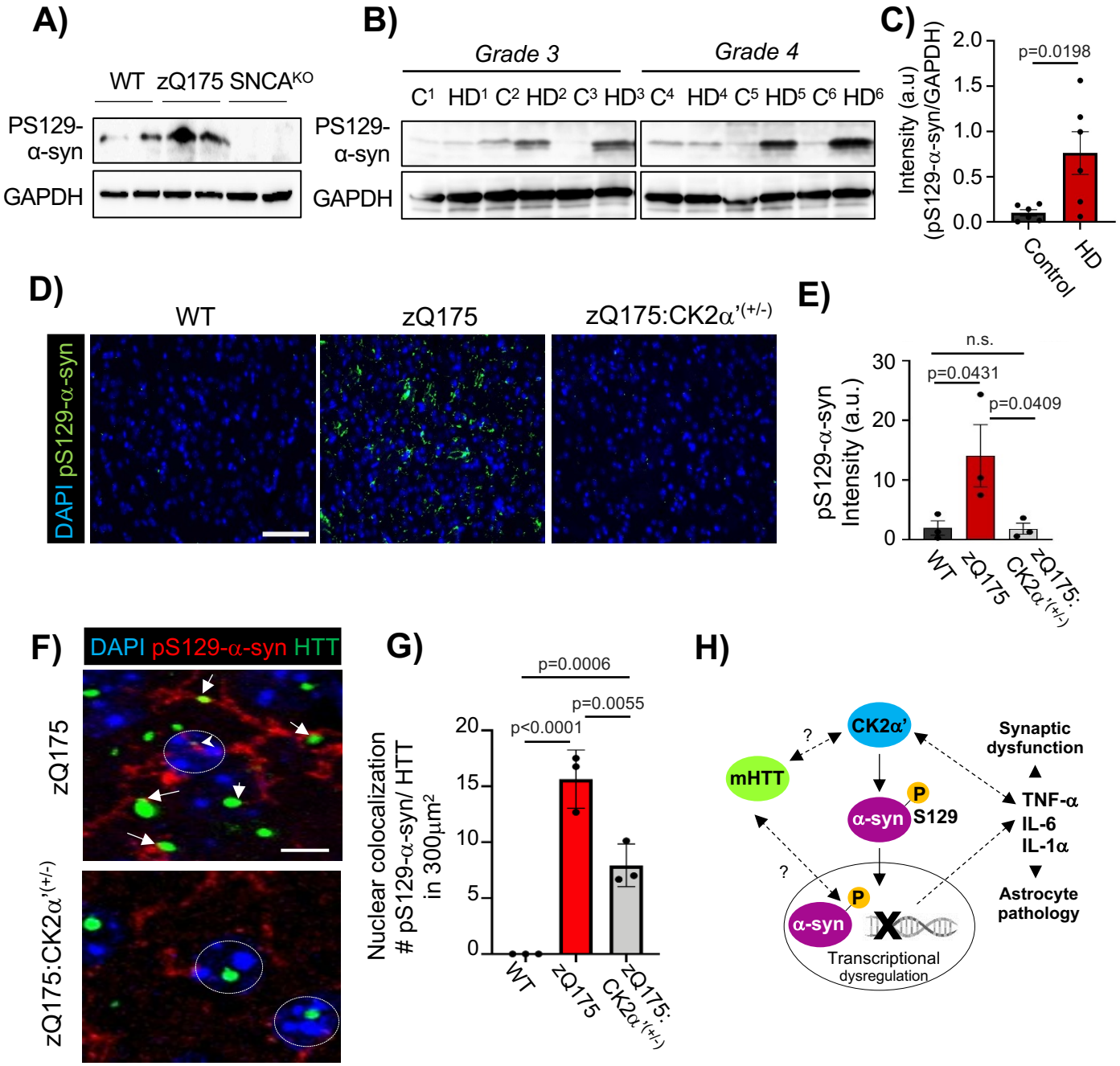
A)
WT zQ175 SNCA^KO
PS129-α-syn
GAPDH
B)
Grade 3
Grade 4
C1 HD1 C2 HD2 C3 HD3 C4 HD4 C5 HD5 C6 HD6
PS129-α-syn
GAPDH
C)
Intensity (a.u) (pS129-α-syn/GAPDH)
p=0.0198
Control
HD
D)
WT
zQ175
zQ175:CK2α'(+/-)
DAPI pS129-α-syn
E)
pS129-α-syn Intensity (a.u.)
n.s.
p=0.0431
p=0.0409
WT
zQ175
zQ175: CK2α'(+/-)
F)
DAPI pS129-α-syn HTT
zQ175
zQ175:CK2α'(+/-)
G)
Nuclear colocalization # pS129-α-syn/ HTT in 300μm²
p=0.0006
p=0.0055
p<0.0001
WT
zQ175
zQ175: CK2α'(+/-)
H)
CK2α'
mHTT
α-syn
P
S129
Synaptic dysfunction
TNF-α
IL-6
IL-1α
Astrocyte pathology
Transcriptional dysregulation

Figure 8